SOLAR WIND:

DETECTION METHODS AND

LONG-TERM FLUCTUATIONS

JARI VILPPOLA

UNIVERSITY OF OULU
REPORT SERIES IN PHYSICAL SCIENCES
Report No. 26 (2003)

SOLAR WIND:

DETECTION METHODS AND

LONG-TERM FLUCTUATIONS

JARI VILPPOLA

Department of Physical Sciences
University of Oulu
Finland

Academic dissertation to be presented, with the permission of the Faculty of Science of the University of Oulu, for public discussion in Kuusamonsali (Auditorium YB210), Linnanmaa, on 22 November, 2003, at 12 o'clock noon.

REPORT SERIES IN PHYSICAL SCIENCES Report No. 26

OULU 2003 ● UNIVERSITY OF OULU

Copyright © 2003
University of Oulu, 2003

ISBN 951-42-7195-5 (URL: http://herkules.oulu.fi/isbn9514271955/)

ALSO AVAILABLE IN PRINTED FORMAT
Report Series in Physical Sciences, Report No. 26, 2003
ISBN 951-42-7194-7
ISSN 1239-4327 (URL: http://herkules.oulu.fi/issn12394327/)

Oulu University Press
Oulu 2003

Vilppola, Jari, Heikki,
Solar Wind: Detection Methods and Long-term Fluctuations

Department of Physical Sciences, University of Oulu, Finland.
Report No. 26 (2003)

Abstract

The Cassini/Huygens mission is a collaborative mission of NASA and ESA to study the Saturnian system. Cassini Plasma Spectrometer (CAPS) is one of the scientific investigations onboard the Cassini orbiter. It consists of three separate spectrometers: Electron Spectrometer (ELS), Ion Mass Spectrometer (IMS) and Ion Beam Spectrometer (IBS). The University of Oulu has a co-investigator status in the CAPS project, and been mainly involved in simulating the structure and scientific performance of the IBS instrument. IBS is a high resolution hemispherical electrostatic analyser aimed to study the solar wind ions. This thesis contains an Introduction and five original papers. Papers I-III contain a detailed description of the simulation process of the IBS instrument and related results. In Paper I the manufacturing tolerances were calculated in order to verify that the high resolution requirements can be achieved using available manufacturing processes. In Paper II the simulations have been further developed and the instrument properties have been studied in more detail. In Paper III the simulation model is used to help the analysis and interpretation of the laboratory calibrations of the IBS flight model. Papers IV and V study the long-term fluctuations in solar wind and interplanetary magnetic field in the period range of 1-2 years (so called mid-term quasi periodicities, MTQP), using the wavelet transformation method to produce dynamic power spectra. In paper IV the MTQP structure in solar wind speed at 1 AU was studied using the longest available series of geomagnetic activity. It was shown that the long-term occurrence MTQP fluctuations roughly follows the long-term solar activity, suggesting that MTQP fluctuations are closely connected with the solar dynamo activity. Moreover, it was also noted that MTQP activity may offer a possibility for a precursory signal which could be used to predict significant changes in long-term solar activity. While Paper IV presents the temporally longest study of MTQP fluctuations, Paper V gives the spatially widest treatment of the same phenomenon. Paper V studies MTQP fluctuations in solar wind and interplanetary magnetic field measured by four probes in the outer heliosphere. It is shown that two MTQP fluctuations of different periods (1.3 and 1.7 years) coexisted during solar cycle 22, while during solar cycle 21 only the 1.7-year band existed. This suggests that the solar dynamo acts differently during even and odd cycles. It is also shown that the two MTQP fluctuations during solar cycle 22 are organized latitudinally. While the 1.3-year periodicity originates from equatorial regions, the 1.7-year fluctuations arise at mid-latitudes.

Keywords: Electrostatic analyser, Simulation, Periodicities, Solar wind, Interplanetary magnetic field, Long term fluctuations

Preface

This work has been carried out at the Department of Physical Sciences of the University of Oulu, Finland. I thank professors Rauno Anttila and Jukka Jokisaari, the former and present head of the Department, for placing facilities at my disposal. I would like to express my deepest gratitude to my supervisors prof. Pekka Tanskanen and prof. Kalevi Mursula for their guidance and support during this work. I would like to thank prof. Tuomo Nygren, the present head of the Space Physics group, prof. Jorma Kangas, the former head of the Graduate School in Solar-Terrestrial Physics, as well as the whole Graduate School team for their guidance during my studies. I would like to thank the co-authors Dr. Heikki Huomo, Mr. Jyrki Keisala, Dr. Bruce Barraclough, Dr. David McComas, and Dr. Bertalan Zieger for their help during the work. I also would like to thank those of my colleagues at Los Alamos National Laboratory who have participated in the work even if not mentioned as a co-author. I also would like to thank Dr. David Young, the PI of the CAPS team for his help and comments during the work, as well as the whole CAPS team for their support. I also would like to thank my colleagues, present and former, in the Department of Physical Sciences for offering an excellent working environment. My special thanks go to Dr. Reijo Rasinkangas, Mr. Jouni Jussila, and Mr. Petri Kekkonen for their help in computational matters. I also would like to thank Ms. Leena Kalliopuska for secretarial help. I would like to thank the pre-examiners Dr. Esa Kallio and Dr. Scott Bolton for their competent evaluation and for their valuable comments in order to improve this thesis. I would like to express my gratitude to the Academy of Finland for financing both the Cassini project at the Space Physics group and the Graduate School. I also would like to thank the Faculty of Science at the University of Oulu, Magnus Ehrnrooth Foundation, and Väisälä Foundation, for financial support of this work. Finally, I would like to thank my parents Aili and Timo, my brothers Harri, Vesa, and Pekka, and sister Hanna-Liisa, and her boyfriend Jonny who have helped and supported me very much during this work.

Oulu, November 10, 2003

Jari Vilppola

Original publications

This thesis consists of an introduction and five original papers. Please note that this electronic version does not contain the original papers.

I *J. H. Vilppola, J. T. Keisala, P. J. Tanskanen, and H. Huomo, Optimization of hemispherical electrostatic analyzer manufacturing with respect to resolution requirements, Rev. Sci. Instrum.,* **64***, 2190-2194, 1993.*

II *J. H. Vilppola, P. J. Tanskanen, H. Huomo, and B. L. Barraclough, Simulation of the response function of a plasma ion beam spectrometer for the Cassini mission to Saturn, Rev. Sci. Instrum.,* **67***, 1494-1501, 1996.*

III *J. H. Vilppola, P. J. Tanskanen, B. L. Barraclough, and D. J. McComas, Comparison between simulations and calibrations of a high resolution electrostatic analyser, Rev. Sci. Instrum.,* **72***, 3662-3669, 2001.*

IV *K. Mursula, B. Zieger and J. H. Vilppola, Mid-term quasi-periodicities in geomagnetic activity during last 15 solar cycles: Connection to solar dynamo strength, Solar Phys.,* **212***, 201-207, 2003.*

V *K. Mursula, and J. H. Vilppola, Fluctuations of the solar dynamo observed in the solar wind and interplanetary magnetic field at 1 AU and in the outer heliosphere, Submitted to Solar Phys. in September 2003.*

In the text, original papers are referred to using roman numerals I-V.

Contents

1. Introduction

A new era in science can be said to have started in 1957 when the Soviet Union launched the first man-made satellite, Sputnik-1. This was an equipment which was totally different from its predecessors and in a completely new environment, in open space, but still in the prison of Earth's gravity. Naturally, space science had started much earlier, as demonstrated for example by continuous measurements of geomagnetic activity which began in the 19th century, but Sputnik paved the way to the in situ measurements in space. After Sputnik numerous satellites have been launched to study the near-Earth space. Earth's gravity has been won, other planets have been studied, and the front line of man-made measurements is rapidly traveling with the Voyager 1 and 2, and Pioneer 10 and 11 spacecraft into the outer space - free from the Sun's gravity.

Pioneer 11, Voyager 1 and Voyager 2 spent (in 1979, 1980 and 1981, respectively) a short, but very important moment studying the Saturnian environment. However, as usual in science, the results obtained during these short flybys raised several new questions. Thus NASA, in co-operation with ESA, started to plan a new mission to study the Saturnian environment in more detail. The mission was named according to the Italian astronomer Giovanni Cassini (1625–1712), who found several moons in the Saturnian system, and to Christiaan Huygens (1629–1695) who found the Titan moon in 1655. NASA provided the Cassini Saturn orbiter and ESA provided the Huygens Titan probe.

The space physics group of the University of Oulu led by prof. Pekka Tanskanen decided to participate in the Cassini Plasma Spectrometer (CAPS) investigation aboard the Cassini orbiter. I was lucky to join the team to work with the simulations of the hemispherical electrostatic analyser which was named the Ion Beam Spectrometer (IBS). The first results from this work were published in Paper I in 1993. Subsequent IBS studies led to Paper II and another paper [*Vilppola et al.*, 1998]. Meanwhile the Cassini spacecraft was built and launched to Saturn in October 1997 from Cape Canaveral, in Florida, USA. The above studies were collected and published as part of my licentiate thesis [*Vilppola*, 1998]. When the calibration of the IBS instrument was analysed, the simulation models were further developed. This led to Paper III. In this PhD thesis, Papers I, II and III form the material which can be called Part I of this thesis: The instrument development.

At the moment Cassini is still on its way to Saturn. Although CAPS has already produced some useful data, the official mission will start only in July 2004 when Cassini will arrive to the Saturnian system.

Since IBS is a solar wind sensor, we decided to study the properties of the solar wind as a part of my thesis. Unfortunately, the so called cruise phase science which was part of the original Cassini science program was cut off because of financial constraints. Therefore extensive measurements of solar wind during the cruise phase from the Earth to the Saturn were omitted and no significant data on solar wind was obtained from Cassini. Therefore, we had to use data from other satellites in order to study the solar wind properties. After the finding by *Richardson et al.* [1994] of large 1.3-year fluctuations in solar wind, considerable international interest was given to the so called mid-term quasi-periodicities (MTQP) which cover the period range from one year to two year. This topic was also studied in Oulu in the group led by prof. Mursula and I joined this effort.

In paper IV we used the fact that geomagnetic activity is a very good estimator of the long-term solar wind speed. Thus without actual measurements of solar wind we can indirectly estimate the solar wind conditions if we have measurements available to calculate geomagnetic activity. Such measurements started already in the mid-19th century, extending the interval of direct solar wind measurements by more than 100 years. Naturally the solar wind estimates by geomagnetic activity can only determine the solar wind conditions within $\pm$ 7° of heliospheric latitude at the distance of 1 astronomical unit (AU) where the Earth is located. On the other hand, when we study solar wind properties in other heliospheric locations we are restricted to those, rather few spacecraft measurements that are available from various space missions. Also, spacecraft measurements have their own, specific restrictions. One important issue which restricts the usage of the spacecraft in the fairly long period range that we are interested, is the spatial and temporal mixing of the signal. Thus, e.g., one of the most interesting heliospheric probes, the Ulysses probe, is practically ruled out for our purposes since it travels during one 1-2-year fluctuation such a wide latitude range that spatial and temporal fluctuations are severely mixed. Another heliospheric probe, the Galileo satellite, is ruled out since it spends most of its time inside the Jovian magnetosphere.

Accordingly, the best available data for the study of the occurrence of MTQP in the outer heliosphere come from the old workhorses, Pioneer 10 and 11 and Voyager 1 and 2. During their travel through the solar system they are reasonably stationary, especially in latitude, over the time scale in which we are interested. We have concentrated on the measurements of solar wind speed (V), and the magnitude of the interplanetary magnetic field (IMF B_{tot}) from these probes. As a comparison we use measurements at 1 AU, given in the OMNI data set, a cross-correlated data set of solar wind measurements from numerous Earth orbiting satellites [*Couzens and King*, 1986; *King*, 1977]. Paper V presents our results on MTQP in these two heliospheric parameters observed in outer heliosphere and at 1 AU. Therefore, in this thesis we have the opportunity to study MTQP using the temporally longest geomagnetic activity index data set available, and the widest possible selection of interplanetary probes to cover the largest spatial region available. Thus, Papers IV and V can be called Part II of this thesis: Temporally and spatially extensive

studies of mid-term quasi-periodicities.

In this Introduction of the thesis I first briefly describe the environment studied, the heliosphere, solar wind, and interplanetary magnetic field, as well as discuss the geomagnetic activity. Then I describe the instrumentation used to study MTQP, the plasma spectrometers and magnetometers aboard the Pioneer 10 and 11 and Voyager 1 and 2. Next I describe the Cassini mission and, especially, the CAPS instrument, and the work done within the IBS simulations. Finally I make a brief description of MTQP and give final conclusions.

1.1. Heliosphere

Scherer et al. [2000] gives a good, short definition for the heliosphere: Heliosphere is the space filled by the plasma originating from the Sun. In addition to the Sun and its upper atmosphere, the solar corona, this definition means the whole interplanetary space where the anti-sunward solar wind plasma flow and the frozen-in interplanetary magnetic field are the main physical phenomena. With its varying activity, so called solar activity, the Sun modulates the whole heliosphere via these heliospheric variables. Therefore, in addition to observing the Sun directly, it is also important to study the heliosphere since new, interesting information about the Sun and its phenomena can be obtained thereby, as described in Papers IV and V. While solar activity covers a wide range of phenomena and time scales, one of the main reasons to study MTQP range fluctuations in the outer heliosphere was, in addition to the above mentioned observation by *Richardson et al.* [1994], the discovery of 1.3-year oscillations in the deep solar convection layer [*Howe et al.*, 2000] from helioseismic studies.

On the far end in the outer heliosphere is first a heliospheric shock called the termination shock, where the solar wind is decelerated to a subsonic value before facing the plasma from the interstellar space. (A nice overview of the outer heliosphere is given in *Suess* [1990]). The region beyond the termination shock which contains plasma both from the Sun and the interstellar space is called the inner heliosheath, ending at the heliopause. Outer heliosheath is between the heliopause and the heliospheric bow shock which is formed where the interstellar plasma faces the obstacle formed by the plasma pressure from the Sun. Beyond the bow shock the interstellar plasma is undisturbed. The heliosphere also contains a heliotail in the the direction opposite to where the solar system is moving in the interstellar plasma.

The distance of the termination shock is estimated to be about 100 AU. This distance varies with the plasma pressure of the solar wind as well as possible variations of the interstellar pressure. Voyager 1 and 2 and Pioneer 10 and 11 probes are currently traveling in the region where the first evidence for the termination shock has been obtained (Munakata et al., rapporteur talk in cosmic ray conference, 2003). For a review of the instrumentation available to study the properties of the termination shock, see *Pesses et al.* [1993]. Voyager 1 is now (Fall 2003) traveling at the distance of 90 AU from the Sun and Voyager 2, Pioneer 11 and Pioneer

10 at 71 AU, at 64 AU and at 84 AU, respectively. Pioneer 11 delivered useful data last time in 1994, and Pioneer 10 in 1998. Voyagers are still operational. Pioneer 10 has lost its connection with the Earth but the other three are still active, and can be used, e.g., to study the transition regions between solar wind and interstellar matter. The neutral atoms in the interstellar space do not face the heliospheric shocks and can traverse into the inner heliosphere until solar UV radiation or collisions with the solar wind plasma ionize them. Thereafter they are called pick-up ions. The pick-up ions have been observed for example with the CAPS instrumentation. After pick-up ions have move with the solar wind to the termination shock they may be accelerated there to considerable energies. Thereafter they may be observed even at 1 AU as anomalous cosmic rays.

1.2. Solar wind

The solar wind is a continuous flow of plasma from Sun. It contains electrons and protons, but also heavier nuclei like alpha particles as minor species. Some of the most abundant heavy elements are oxygen, carbon, iron, silicon, neon, nitrogen, magnesium, and argon [*Gosling*, 1999] which appear in several isotopes, as well as in several ionisation levels. The first indirect evidence that something invisible was flowing out from the Sun was noted when the origin of cometary tails was considered (See the historic review by *von Steiger* [Submitted 2002]). Also auroras were long considered to be driven by the solar wind. The first theoretical treatment for a continuously blowing solar wind was given by *Parker* [1958], who extended the theoretical work of *Chapman* [1957] that the solar corona is extending out to interplanetary space.

Solar wind can roughly be divided into a slow wind and a fast wind. The slow wind comes from streamer belts, areas of closed magnetic field lines in the Sun. The slow solar wind speed is around 250–400 km/s, and its density is around 11 cm^{-3} at 1 AU. The high speed solar wind is flowing from coronal holes, large areas of open magnetic field lines. The speed of the fast solar wind is around 400–800 km/s [*Cranmer*, 2002] and the density is around 3 cm^{-3}, i.e., lower than in the slow speed stream. The average helium content is slightly higher in the fast wind than in the slow wind ($\sim$3.6% versus $\sim$2.5%). In addition to the heavy elements occurring in the solar atmosphere, the solar wind interaction with planetary atmospheres and other bodies in the solar system produces small amounts of heavier compounds detectable in the distant solar wind.

During the solar cycle minimum times the magnetic field of the Sun is well organized, and the dipole approximation for the magnetic field is well justified. The coronal holes are located around the polar caps, and the high speed streams dominate the mid- and high latitudes. Occasionally the Earth faces these high speed streams but more often the Earth is in the streamer belt and in the low speed solar wind. During the solar minimum times the heliospheric current sheet is rather flat. (The so called ballerina skirt is flapping only weakly). During the solar maximum times the magnetic field of the Sun is very disturbed and far from

the purely dipolar structure. While the large polar coronal holes disappear during the ascending phase of the solar cycle, smaller and shorter living coronal holes can appear during the solar maximum at all latitudes, including the equatorial region. However, only few of these coronal holes are sufficiently large or persistent in order to significantly affect the solar wind properties. Therefore the solar wind during the maximum times is generally dominated by the slow solar wind which is emitted from the many streamer belts that may coexist all over the solar surface during solar maximum. After the maximum the polar coronal holes reappear but the polarities of the magnetic field in the two caps are interchanged, corresponding to the reversal the direction of the global magnetic field during the solar maximum. (A detailed description of the polar field reversal during cycles 21 and 22 is given in *Fox et al.* [1998]). During the declining phase of the solar cycle the polar coronal holes often tend toward the solar mid-latitudes, leading to a strongly tilted streamer belt and helioshperic current sheet. Such a period is called the excursion phase and leads to a strong variation of solar wind properties either once or twice during one solar rotation of about 27 days (for a review see, e.g., *Mursula and Zieger* [1996]). It has also been shown [*Mursula et al.*, 2002] that during the declining phase and minimum the streamer belt is systematically displaced from the equator, which means that the heliosphere is north-south asymmetric at these times.

Since the coronal holes are the source of the fast solar wind the properties of the coronal holes have a strong influence on the solar wind in the different locations of the heliosphere. For example, strong MTQP range (1.7 year) fluctuations have been observed in the coronal hole area of the southern solar hemisphere for many years around 1980 [*McIntosh et al.*, 1992]. This periodicity also affects the the near and distant heliosphere, modifying the properties of the solar wind and the interplanetary magnetic field, as well as other parameters dependent on them. An example of the latter are the galactic cosmic rays, where a similar 1.7 year periodicity has been observed [*Valdes-Galicia et al.*, 1996]. Our studies in Paper V also show that the same periodicity is present in the solar wind speed and also in the IMF magnitude in different locations around heliosphere.

Above we have considered the solar wind in a simple two-phase model with a fast and slow wind component. Of course, the true situation is much more complex than this. Naturally, when these two components co-exist in the heliosphere they also interact with each other. The fast wind, catching up the slow wind, pushes the slow wind ahead, and solar wind is compressed. This creates a region with strong perturbations and shocks. Ahead of this region is the forward shock and behind the reverse shock. The same coronal hole structure in the Sun typically prevails during several solar rotations, creating repeated patterns of slow and fast solar wind streams and superficially co-rotating shock regions between them which can be repeated during several solar rotations. Therefore these shock regions are called co-rotating interaction regions (CIR) [*Gazis*, 1996b; *Gosling*, 1999]. When studying CIRs and other heliospheric structures out of the equator, the Ulysses probe is a best available equipment (see, e.g., *Gosling* [1996]). In addition, the outer heliospheric probes Voyager 1 and 2 have been used to study the latitudinal structure of these phenomena [*Kane et al.*, 1998]. Further out from the Sun the

solar wind may become even more complex. Two separate CIRs may coalesce and produce one larger shock phenomenon called the merged interaction region (MIR) (for a review, see *Gazis* [1991]).

There are also other phenomena which complicate the above described simple two-phase model of the solar wind. The most significant of these are the coronal mass ejections (CME) [*Gosling*, 1990, 1997]. CMEs originate from regions of close magnetic field structures which may break and release large amounts of coronal matter into space. Therefore the solar wind density during a CME is clearly higher than the average solar wind density. However, the solar wind speed in the CME can be either extremely low <300 km/s or extremely high >1000km/s. The solar/IMF magnetic field structure also changes dramatically during a CME. The field lines of the CME may either remain rooted in the Sun, or create a region of closed field lines, detached from the Sun. In the former case a spiral magnetic structure called the magnetic flux rope is created, the latter case of the closed field line region is called the magnetic cloud. CMEs are mostly responsible for geomagnetic storms, since CMEs both have a strong magnetic field, especially the southward component is important, and a high solar wind pressure (see, e.g., *Gosling* [1993]). Although the temporal scale of CMEs and CIRs is much shorter than the MTQP time scale, they may have a notable influence by modifying the long-term properties of the solar wind and IMF. However, a detailed study of these effects is left beyond this thesis.

1.3. Interplanetary magnetic field

The magnetic field of the Sun is produced in a dynamo process at the bottom of the differentially rotating convection zone at the distance of about 0.7 solar radii from the solar center. Below the convection zone is the uniformly rotating solar interior with the radiative zone. The transition region between the radiative and convection zones is called the tachocline. The first detection of Sun's magnetic field was made by *Hale* [1908] when he noted using the Zeeman effect that magnetic fields in sunspots are about 2000–3000 gauss [*Parker*, 2001]. The solar magnetic field experiences a cyclic process with a 22-year period during which the Sun goes through two solar minima with a roughly north-south oriented dipole like magnetic field and two maxima with a highly disturbed magnetic field when the main dipole may be tilted up to 90° [*Wang et al.*, 2000]. During maximum the total field of the Sun change its polarity, and has a multi pole structure rather than a simple dipole. (Strictly speaking, the magnetic field structure is also affected by the induced field of the current sheet). The above mentioned solar activity cycle is 11 years long, i.e., one half of the total magnetic cycle, and was known already long before the full 22-year magnetic cycle was recognized. However, it is also known that the solar cycle length may vary from cycle to cycle (see, e.g., *Fligge et al.* [1999]).

In a highly conductive plasma flow the magnetic field diffusion is negligible and the magnetic field lines travel along with the plasma flow - the magnetic field is frozen-in to the plasma flow. The frozen-in concept was introduced by the Nobel

physicist Hannes Alfvén. (For more details see, e.g. *Koskinen* [2001] or *Kivelson and Russell* [1995]). The solar wind flow is highly conductive and thus it is safe to conclude that in the heliosphere the magnetic field is frozen-in to the solar wind flow. The Sun is rotating with a typical mid-latitude period of about 27 days. These two features lead to so called Parker spiral structure [*Parker*, 1958] where the magnetic field lines have a form of an Archimedean spiral. This structure implies that the magnetic field lines at the Earth's orbit form an angle of about 45° with solar direction. In the very far heliosphere this angle approaches 90°. The following equations give the radial dependence of the magnetic field components at the equator according to this model:

$$B_R(R) = B_{R0}\frac{R_0^2}{R^2}, \tag{1.1}$$

$$B_\phi(R) = B_{R0}\frac{R_0^2\Omega_S\cos\theta}{RV} = B_{\phi 0}\frac{R_0}{R}, \tag{1.2}$$

and

$$B(R) = B_0\frac{R_0^2}{R^2}\left(\frac{1+(\Omega_S R\cos\theta/V)^2}{1+(\Omega_S R_0\cos\theta/V)^2}\right)^{1/2} \tag{1.3}$$

In these equations B_R denote the radial component of the interplanetary magnetic field, B_ϕ its azimuthal component, and B its magnitude. R is the distance from the Sun, R_0 is the distance from the Sun at some reference point (like the Earth), Ω_S is the angular frequency of solar rotation, V is the solar wind speed, and θ the heliographic latitude. As can be seen from these equations, the variation in solar wind speed has an influence on the Parker spiral angle.

The situation out of the ecliptic is more complex than given in the above equations. Because of the flux tube expansion the magnetic field line can have a foot-point at a higher latitude on the Sun [*Wang and Sheeley*, 1990]. Also, the Sun is rotating differentially and the solar surface has slower rotation speed at high latitudes than at the equator. It has to be noted also that temporary phenomena like flux ropes and magnetic clouds with complex magnetic loop structures may disturb the average heliospheric field locally. Thus the local field might be very far from the ideal Parker spiral model which only gives an average structure for the interplanetary magnetic field.

1.4. Geomagnetic activity

Geomagnetic activity describes the magnetic disturbances measured at the Earth's surface. Regular magnetic measurements started already in the mid-19th century. Even earlier, since late 16th century, magnetic phenomena were already studied scientifically, and the Earth's magnetic field was measured occasionally. When the number of continuously measuring magnetic stations increased, this gave the opportunity to calculate indices which describe the global disturbance level. These indices are generally called geomagnetic activity indices. Different indices have

been calculated from stations that are located in areas influenced by different phenomena in the Earth's magnetosphere and ionosphere. For example, the auroral electrojet (AE) index is based on measurements at high (auroral) northern latitudes while the ring current (Dst) index uses stations located at low latitudes. The longest uniform index of geomagnetic activity (from 1868 to present) is formed by the aa index series developed by *Mayaud* [1972, 1973]. By combining the aa index with the measurements at the Helsinki magnetic-meteorological observatory (see, e.g., [*Nevanlinna and Ketola*, 1993]), *Nevanlinna and Kataja* [1993] could extend the aa series to cover solar cycles 9 and 10. The aa_{Hel} series overlaps with Mayaud's aa index from 1868 to 1880. For monthly mean values the correlation coefficient between the two is 0.96. Therefore the extension of the aa series by aa_{Hel} data can well be accepted, forming the longest continuous index of geomagnetic activity from 1844 to present. In Paper IV we have used this series to study the properties of mid-term periodicities over centennial times scales.

Although the aa index is based only on two mid-latitude stations, it describes very reliably the long-term behavior of global geomagnetic activity. This can be verified by comparing it with other indices that are based on a larger number of mid-latitude stations, such as the Kp and Ap indices. E.g., the annual averages of the Ap and aa indices were found to correlate very well with each other over several decennia [e.g., *Crooker and Gringauz*, 1993; *Rangarajan and Barreto*, 2000]. While the mid-latitude stations are most suitably located to measure the total effect on geomagnetic activity by different current systems, the high-latitude stations are dedicated to measure the currents in the high-latitude ionosphere and the field-aligned currents. Moreover, the AE index is sampled every 5 minutes while the mid-latitude indices are typically 3-hour indices. Despite these differences, the high-latitude AE index correlates very well with the aa index when using annual averages [*Stamper et al.*, 1999]. Thus the selection of stations involved in the compilation and the method of compilation of the index is not very important when considering the level of geomagnetic activity averaged over times of about one year or longer.

Several studies have been made in order to find out what factors in solar wind and interplanetary magnetic field cause geomagnetic activity. The Ap index was found to correlate quite well both with solar wind speed squared (V^2) (correlation coefficient = 0.86) and with B_sV^2 (c.c. = 0.90) during solar cycle 20 [*Crooker et al.*, 1977]. Here B_s is the southward directed component of the interplanetary magnetic field (B_s=-B_z when $B_z <= 0$ and B_s=0 elsewhere). *Crooker et al.* [1977] noted that the B_s-term controls the product B_sV^2 at hourly time scales while the V^2 term controls it at annual time scales. This suggests that the Ap index, i.e., geomagnetic activity is driven by the B_sV^2 term over short time scales and by the V^2 over long (e.g., annual) time scales. However, in subsequent studies [*Crooker and Gringauz*, 1993], it was found that during the next solar cycle 21 the correlation of the Ap index with B_sV^2 remains high (c.c. = 0.90), but correlation with V^2 drops (c.c. = 0.62). They noted that the B_s-term also has a contribution to the correlation with geomagnetic activity in annual time scales outside the solar cycle 20. The correlation coefficient for annual means between the aa-index and B_sV^2 (V^2) from 1964 to 1996 was 0.87 (0.66). *Stamper et al.* [1999] noted that

correlation decreased when solar cycle 22 was included in the analysis. *Schreiber* [1998] has also studied the B_s and V^2 terms separately during solar cycle 21, finding that V^2 dominates in the declining phase but B_s in the ascending phase of the solar cycle. The polar coronal holes have their largest extension toward the equator during the declining phase of the solar cycle, allowing high speed solar wind streams to be observed at low latitudes and compressing the heliospheric current sheet flat. This enhances the significance of the V^2 term and limits the north-south fluctuations of IMF. During the ascending phase polar coronal holes quickly disappear and the heliospheric current sheet becomes more curved. This allows stronger fluctuations in the north-south component of IMF, and enhances their significance for geomagnetic activity.

Stamper et al. [1999] studied several interplanetary coupling functions and found the best correlation with the annual means of the *aa*-index and the coupling functions

$$P_m = \langle M_E \rangle^{2/3} \langle N_{sw} \rangle^{(2/3-\alpha)} \langle V \rangle^{(7/3-2\alpha)} \langle B_{tot} \rangle^{(2\alpha)} \left\langle \sin^4 (\theta/2) \right\rangle \tag{1.4}$$

and

$$\langle P_m \rangle = \left\langle M_E^{2/3} N_{sw}^{(2/3-\alpha)} V^{(7/3-2\alpha)} B_{tot}^{(2\alpha)} \sin^4 (\theta/2) \right\rangle . \tag{1.5}$$

In the function 1.4 annual means of each component are calculated first and then multiplied to get the coupling function. In the function 1.5 the value of the coupling function is first calculated from hourly means of each component and these values are then averaged to annual means. M_E is the magnetic moment of the Earth, N_{sw} is the solar wind density, V is the solar wind speed, B_{tot} is the intensity of the interplanetary magnetic field, θ is the so called IMF clock angle (angle between Z-axis and IMF direction projected in the Y-Z plane; positive from Z-axis to Y-axis) in the GSM frame of reference and α is a coupling exponent to be determined. The coupling functions in 1.4 and 1.5 contain most of the energy transfer function for viscous coupling between solar wind and magnetosphere introduced by *Vasyliunas et al.* [1982]:

$$P_\alpha = \{k\pi/2\mu_0^{(1/3+\alpha)}\} m_{sw}^{(2/3-\alpha)} M_E^{2/3} N_{sw}^{(2/3-\alpha)} V^{(7/3-2\alpha)} B_{sw}^{(2\alpha)} \sin^4 (\theta/2). \tag{1.6}$$

Here k is a dimensionless constant and m_{sw} is the mean ion mass of the solar wind, which is roughly constant. *Stamper et al.* used the OMNI data set [*Couzens and King*, 1986; *King*, 1977] in 1964-1996 to provide the measurements of the IMF and the solar wind parameters. While this data set is considered to be very reliable and has been used for many studies, some concern is caused by the fact that data prior and after 1974 cannot be cross calibrated. This may have an influence to the analysis of the whole data set. The best correlation for the whole data set is achieved when coupling exponent has a value $\alpha = 0.386$. The correlation coefficient is then 0.938 for both functions 1.4 and 1.5. *Stamper et al.* also calculated the annual averages of the *aa*-index using only those intervals when OMNI data set had simultaneous data. This excluded nearly 50% of the *aa* values and increased the correlation coefficient up to 0.95. Moreover, by excluding the data before 1974, in view of the cross calibration problem, the correlation coefficient increased to 0.97 with the best coupling exponent being $\alpha = 0.31$. Such a high correlation

means that 93% of the variation in the annual means of the *aa*-index is caused by the interplanetary conditions expressed by the relations 1.4 and 1.5.

When comparing the coupling functions 1.4 and 1.5 with the ones discussed earlier (V^2 and B_sV^2) some details can be noted. The coupling exponent $\alpha = 0.386$ means that the power of solar wind speed in the relations 1.4 and 1.5 is 1.56, which has to be compared with the power 2 in the terms B_sV^2 and V^2. Similarly, the power of the IMF intensity is 0.77 in 1.4 and 1.5, in comparison with power 1 in B_sV^2 and 0 in V^2. Also, the dependence on IMF direction is greatly changed from B_s to $\sin^4(\theta/2)$, the latter allowing even northward directed IMF field to cause geomagnetic activity. The formulas 1.4 and 1.5 also include the dependence on solar wind density so that its power is changed from earlier 0 to 0.28. *Stamper et al.* also synthesized an annual *aa* index from the OMNI data using the regression of $\langle aa \rangle$ with P_m, finding that the predicted *aa*-index correlated with the actual *aa*-index extremely well except that during the first solar cycle studied, solar cycle 20, a few data points deviate from each other.

2. Instrumentation

2.1. OMNI data

Nearly continuous measurements of the solar wind and interplanetary magnetic field at 1AU started in early 1960s. These data have been collected into the public OMNI data base [*Couzens and King*, 1986; *King*, 1977] which includes the values of most heliospheric parameters at the temporal resolution of one hour. This data set contains cross calibrated measurements from several Earth orbiting satellites, providing the best available data set to study the interplanetary conditions during the whole time interval of direct *in situ* measurements. However, it has to be noted that cross calibration is not possible between the early part of the interval (1963–1972) and the later part from 1973 onwards. Also, while the overall data coverage is more than 60 %, there are a number of lengthy intervals with a very low data coverage or no data at all (data gaps). Some of these intervals also affect the interpretation of mid-term periodicities in solar wind in 1970s, as studied in detail in *Mursula and Zieger* [2000]. The OMNI data contain data from the following spacecrafts: IMP 1, IMP 2–8 (also called Explorer 18, 28, 34, 41, 43, 47, and 50), AIMP 1 and 2 (called also Explorer 33, 35), HEOS 1 and 2, VELA 3, OGO 5, ISEE 1–3, PROGNOZ 10, and WIND. Note also that in this thesis we have only used the original OMNI (or OMNI 1) database. An improved OMNI 2 database was published recently. However, all the data analysis for this thesis was already completed before OMNI 2 data base set freed. Therefore only the earlier version of the data base was used here.

2.2. Pioneer 10 and 11

The two Pioneer spacecraft were launched in 1973. There are 11 scientific instruments traveling onboard these spacecraft. Pioneer 10 flied to the Jupiter system and was then deviated out of the ecliptic plane by the Jovian gravitational force. Pioneer 11 first encountered with Jupiter, then with Saturn, and was thereafter

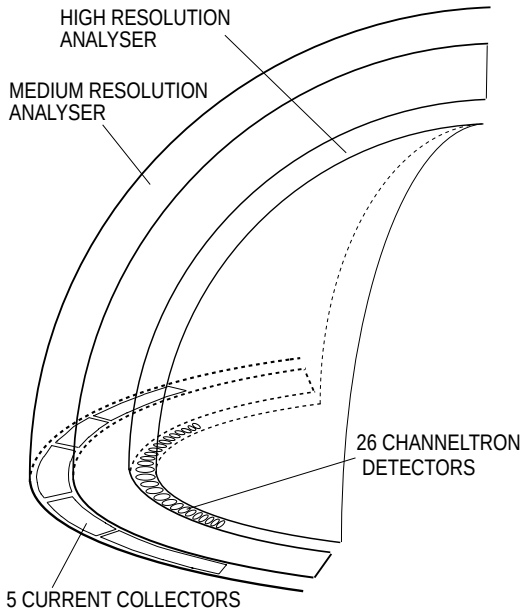

Fig. 2.1. Schematic view of the analyzer and detector portions of the Pioneer plasma analyzer. (See also *Wolfe et al.* **[1974]).**

directed away from the ecliptic plane. During their long flight in the interplanetary space these two spacecraft have collected a significant amount of solar wind and IMF data by the plasma spectrometers and magnetometers. Pioneer spacecraft are spin-stabilized, rotating around their Z-axis which points through the high gain antenna normal towards the Earth.

2.2.1. Pioneer Plasma Spectrometers

The PI of the plasma instruments in Pioneer 10 and 11 is Dr. Aaron Barnes from Ames Research Center. The instruments contain dual 90° quarterspherical electrostatic analysers with multiple charged particle detectors and supporting electronics (see Figure 2.1 for a structural view of the plasma instrument.) The energy range for protons is 100-18000 eV and for electrons 1-500 eV. The inner part of the dual analyzer forms the high resolution analyzer and the outer part the medium resolution analyzer. The analyser constant (energy of accepted charged particles per unit charge divided by the analyser plate potential) of the high resolution analyser is 9. The high resolution analyser has a plate mean radius of 9 cm and 0.5 cm separation. It uses 26 channel electron multiplier (CEM) detectors

to detect the transmitted ions. The CEMs are arranged in a semicircle and they cover the angular range of $\pm 51^\circ$ with respect to the entrance aperture normal. The angular separation is $\sim 3^\circ$ near the central partition of the analyzer, and $\sim 8^\circ$ at the extremes of the analyzer. The energy resolution is $\Delta(E/Q)/(E/Q) = 0.07$.

The medium resolution analyzer has a plate mean radius of 12 cm and 1.0 cm separation. The analyser constant of the medium resolution analyzer is 6. The medium resolution analyzer is used for both electron and ion detection. It contains five flat-surface current collectors. Each of the three central current collectors has a 15° field of view width, and covers an angular range of $\pm 22.5^\circ$ with respect to entrance aperture normal. (Thus the angular ranges are: -22.5° – -7.5°, -7.5° – +7.5°, and +7.5° – +22.5°). The two outermost collectors have an angular width of 47.5°, and they are located at $\pm 46.25^\circ$ with respect to the center of the analyzer. (Thus the angular ranges are: -70° – -22.5° and +22.5° – +70°).

The plasma analyzers in Pioneer spacecraft are mounted so that the entrance aperture normal is parallel with the spin axis which points toward the Earth (practically also toward the Sun), therefore being also parallel to the solar wind flow. There is a specific slit for the plasma instrument in the reflector of the high gain antenna. The edges of antenna reflector limit the instrument viewing to $\pm 73^\circ$. During one rotation of the spacecraft almost one half of the sky is covered. The detailed description about the plasma instrumentation aboard Pioneer 10 and 11 can be found in *Wolfe et al.* [1974] and *Frank et al.* [1980].

2.2.2. Pioneer Magnetometers

The vector helium magnetometer was selected for the Pioneer 10 and 11 missions. The PI of the magnetometers is Dr. Edward J. Smith from Jet Propulsion Laboratory (JPL). The magnetometer contains a helium lamp, a circular polarizer, a helium absorption cell, Helmholtz coils, a lens and an infrared detector. The operation of the instrument is based on the fact that the magnetic field direction affects when the metastable helium is optically pumped. The presence of the ambient magnetic field causes a sine wave modulation of the infrared radiation passing through the helium cell at the fundamental frequency of the applied circular sweep field. The sensor output consists of the nulling currents that remove the effect of circular sweep field. The magnetometer can measure the three magnetic field components in frequency range from 0 to 10 Hz. The magnetometer has eight operation ranges, of which one is selected automatically. The accuracy is at best 0.015γ (15pT), and the highest measurable field magnitude is 1.37G (0.137mT). The sensor is located on a 5 m long boom, 7 m apart from the center spin axis. At the sensor location the magnetic field caused by the spacecraft is estimated to be $<=0.01\gamma$ which is less than the instrument sensitivity and thus negligible. More details about the magnetometers aboard Pioneer 10 and 11 can be found, e.g., in *Smith et al.* [1974].

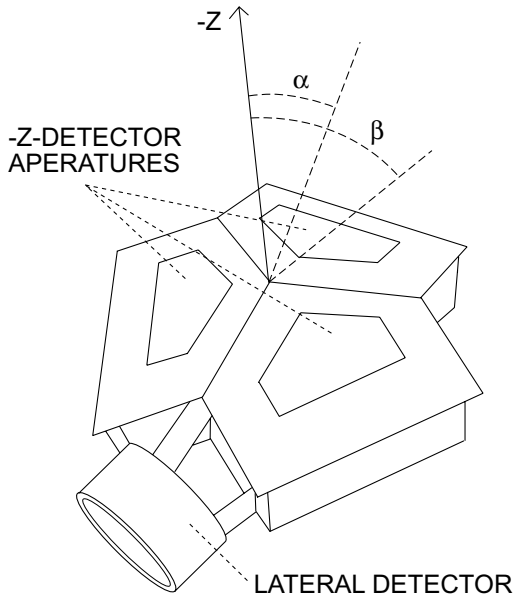

Fig. 2.2. Sketch of the Voyager PLS instrument. The angle α gives combined full view of the three -z-detectors, and angle β the partial view of the individual -z-detector. (Sketched from photograph in *Bridge et al.* [1977]).

2.3. Voyager 1 and 2

The Voyager spacecraft were launched in 1977. There are 11 scientific instruments traveling onboard both spacecraft [*Kohlhase and Penzo*, 1977]. The two spacecraft flied practically on the same trajectory first to Jupiter and then to Saturn, where Voyager 1 was directed out of the ecliptic plane to fairly high heliolatitudes, while Voyager 2 continued to Uranus and Neptune and was only then directed off the ecliptic. As the two Pioneers, the Voyagers have also collected large amounts of solar wind and IMF data during their flight in the interplanetary space. Contrary to Pioneers, the two Voyagers are three-axis stabilized spacecraft.

2.3.1. Voyager Plasma Spectrometers

The PI of the Voyager plasma spectrometer (PLS) is Prof. John W. Belcher from the Massachusetts Institute of Technology. The PLS consists of two separate units of Faraday cup plasma detectors. The Earth pointing -Z unit contains three Faraday cups, and is roughly directed toward the solar wind flow (see Figure

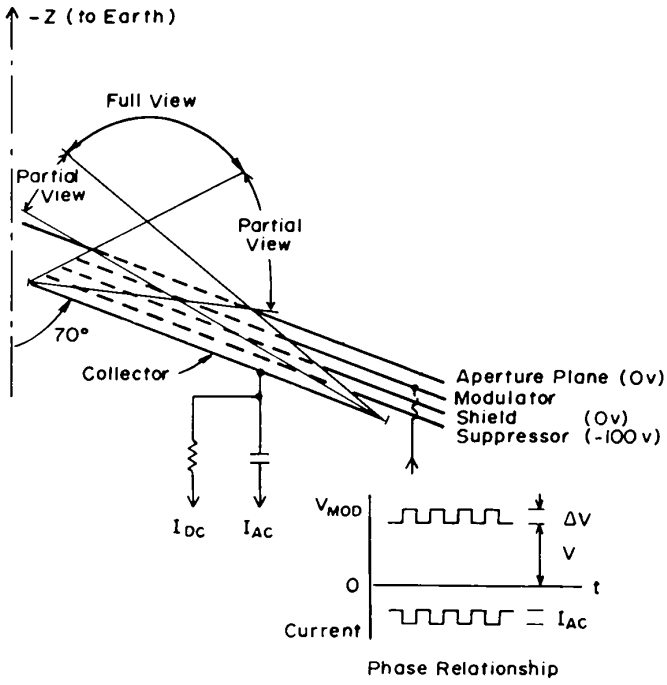

Fig. 2.3. A cross sectional view of the one of the three -Z-detectors of the Voyager PLS instrument (from *Bridge et al.* **[1977]).**

2.2). Each Faraday cup contains an aperture plane, a modulator, six shield grids against secondary electrons, a suppressor and a collector plane (see Figure 2.3), all assembled in a parallel plane, which is 20° tilted from the plane normal to the -Z axis. Thus the three Faraday cups plates of this unit construct a low tetrahedron. The full view when the Faraday cup collector is fully exposed to the solar wind flow is about 45°. The partial view of one Faraday cup is about 75° (see also Figure 2.3). When the partial views from all of the three Faraday cups are combined, the -Z unit covers almost the whole -Z-pointing hemisphere. The other, lateral detector unit, contains only one Faraday cup, and it is designed to point approximately towards the corotating flow during planetary encounters. The Faraday cup is conventional type, and it contains a single collector plate and eight grids. The six grids are electrostatic shields or they suppress secondary electrons and the two are used to select the energy per charge range for positive or negative ions.

The PLS contains several modes with different energy resolutions ($\Delta E/E$ from 3.6% to 100%). The energy range for protons and electrons in the all four Faraday cups is from 10 to 5950 eV. The PLS is assembled on the science scan platform. The platform provides larger field-of-views (FOV) for attitude stabilized

spacecraft. However the technique used in the spectrometers provides solar wind measurements without scanning, which is an important feature in planetary magnetospheres. The detailed description of the plasma experiment aboard Voyager 1 and 2 is given in *Bridge et al.* [1977]. *Richardson* [1986], and *Lazarus and McNutt* [1983] also discuss the instrument briefly.

2.3.2. Voyager Magnetometers

The PI of the Voyager magnetometers is Dr. Norman F. Ness from Bartol Research Institute. These instruments contain two separate systems of high-field and low-field magnetometer. Both systems contain two identical triaxial fluxgate magnetometers which measure the three components simultaneously. Like in the case of Pioneer magnetometers, the low field system has eight dynamic ranges. The low-field system has the best accuracy of 2.2 mγ (2.2 pT), and the highest field still detectable is 0.5 G (50 μT). The accuracy is naturally lower in the higher field modes. The high field system has only two modes. Its maximum accuracy is 12.3 γ (12.3nT), and highest detectable field 20 G (2.0 mT). In the dual sensor concept the two separate sensors are mounted at different distances on the 13-meter magnetometer boom. Thus the spacecraft magnetic field can also be estimated by the two instruments. The ambient magnetic field can be calculated by subtracting the spacecraft field from the measured total field. A detailed description of the magnetometers aboard the Voyagers is given in *Behannon et al.* [1977].

2.4. Cassini

2.4.1. Introduction

The Saturn orbiter Cassini provided by NASA and the Titan probe Huygens provided by ESA form a natural extension to Saturn science after observations made from Earth during several centuries, and after three short planetary encounters realized by Pioneer 11 in 1979, and Voyager 1 and 2 in 1980 and 1981. Although the spacecraft and probe are provided by ESA and NASA, the High Gain Antenna (HGA) aboard the Cassini orbiter is designed and manufactured by Italian Space Agency. The side view of the Cassini spacecraft with Huygens probe connected to it is presented in Figure 2.4.

The Cassini spacecraft was launched on a Titan IVB booster with Centaur upper stage on 15th of October, 1997, from Cape Canaveral in Florida, USA. After launch, the Cassini headed towards Venus. With the help of Venus' gravity assist in April 1998 the Cassini spacecraft was accelerated further outward into the Solar System. Nevertheless, one gravity assist was insufficient and the spacecraft was turned back into the inner solar system after it had reached the distance of about 1.5 astronomical units (AU) from the Sun in December 1998. (1 AU is the

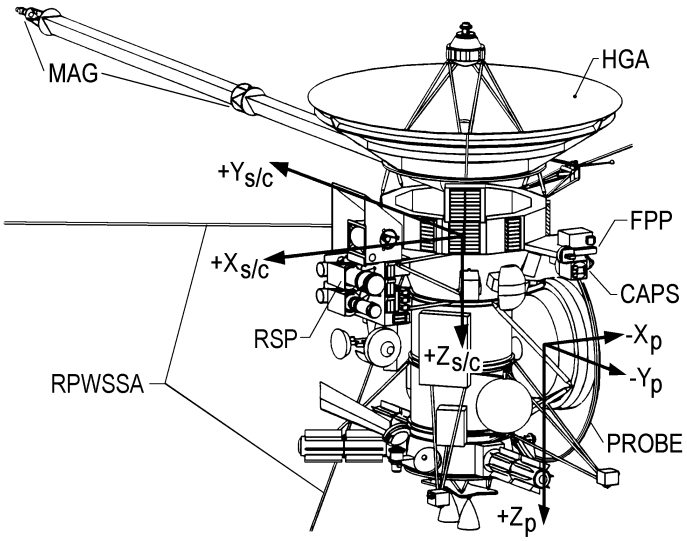

Fig. 2.4. Configuration of the Cassini spacecraft and the Huygens probe. The coordinate systems of the spacecraft $(x_{s/c}, y_{s/c}, z_{s/c})$ and the probe (x_p, y_p, z_p) are given on the figure. Fields and Particles Pallet (FPP), Remote Sensing Pallet (RSP), Cassini Plasma Spectrometer (CAPS), Dual Technique Magnetometer (MAG), Radio & Plasma Wave SubSystem Antenna (RPWSSA) and High Gain Antenna (HGA) are also marked on the figure. (The figure is slightly modified from the original published by *Young and Jensen* **[1993].)**

average distance between the Earth and the Sun). At 1.5 AU a maneuver was required in order to redirect the spacecraft towards Venus. The spacecraft met Venus again in June 1999, and was slung towards Earth by Venus gravity. Earth was attained after two months in August 1999 and with the help of the Earth's gravity assist the spacecraft was directed towards Jupiter. Cassini reached Jupiter in December 2000. The fourth and last planetary gravity assist finally slung the spacecraft towards Saturn. Four years after Jupiter flyby Cassini will arrive at Saturn and will be inserted to an orbit around Saturn on the first of July, 2004.

The arrival at Saturn will be one of the most critical moments during the Cassini mission. During the Saturn encounter the spacecraft will be decelerated using its main engine, so that the spacecraft will be set to an orbit around Saturn instead of continuing on a flyby orbit similar to Venus, Earth and Jupiter encounters. The maneuver must be made automatically, since the control signal from the Earth reaches the spacecraft at the vicinity of Saturn with a delay of more than one hour. The Huygens probe will be released during the third Titan flyby in the January 2005 to investigate the atmosphere and surface of Titan. The orbiter will

operate as a radio link between the Earth and the probe as long as the probe is operational. After the Huygens landing, the Cassini orbiter will continue the mission, investigating the Saturnian environment in detail during the four years long official mission. Currently there are plans that the mission could be continued optional two years.

During the travel from Earth to Saturn the Cassini instruments have already produced data during the last three (second Venus, Earth and Jupiter) flybys. Measurements were made also before and after Jupiter flyby. The main purpose of these measurements has been the calibration of the instruments, although scientific goals have also been in the plan. The most important scientific result so far have been achieved with the simultaneous measurements of the Galileo spacecraft during Jupiter flyby. This was the first time when two simultaneous spacecraft measurements were made in the Jupiter system.

The University of Oulu is also participating in the Cassini mission, and is a CoI institute in the Cassini Plasma Spectrometer (CAPS). The PI of the CAPS instrument is prof. D. T. Young from Instrumentation and Space Research Division at SwRI, USA. There is also a Finnish contribution in the hardware of the CAPS instrument. VTT automation from Otaniemi, Espoo has manufactured the hemispheres for the hemispherical electrostatic analyser of the Ion Beam Spectrometer (IBS) and the actuator of the CAPS. The Finnish company Rejlers OY has participated in the development of the actuator, which provides the rotation capability of the CAPS instrument. Department of Physical Sciences of the University of Oulu has been involved in the planning of the IBS.

2.4.2. Cassini Plasma Spectrometer

2.4.2.1. Introduction

Different plasma diagnostic instruments have been used for space physics studies (for a review see e.g. *Bame et al.* [1986]). In this section one of the scientific investigations aboard the Cassini spacecraft will be considered in more detail. The CAPS investigation [*Young et al.*, 1989, 1996, 1998, 2003] is planned to address numerous science goals in Saturn's magnetosphere as well as in planetological phenomena such as the atmospheres of Saturn and Titan and the surfaces of the icy satellites and rings. CAPS also investigates the solar wind and interstellar pickup ions. The objective is to characterize accurately the composition and dynamics of plasma within Saturn's magnetosphere, including its interactions with Titan and the icy satellites and rings. CAPS will infer the sources and sinks, the transport and acceleration processes and the global distribution of plasmas in Saturn's magnetosphere, and study magnetospheric plasma interactions with the atmospheres of Titan and Saturn, with Titan's ionosphere and wake, and with Saturn's auroral region. It will characterize plasma processes of planetological interest including icy satellite surface re-processing and the electrodynamics of ring spoke formation [*Young and Eaker*, 1991].

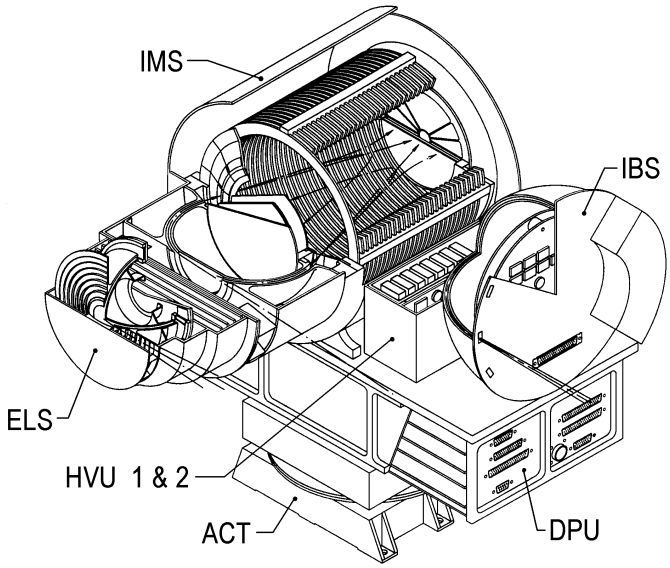

Fig. 2.5. **The cross section of CAPS (from** *Young and Jensen* **[1993]).**

To obtain these scientific objectives CAPS can observe electrons and ion species expected to be encountered during the mission. For example H^+, H_2^+, He^{2+}, N^+, OH^+, H_2O^+ and N_2^+ ions are of great interest, and therefore the CAPS instrument is designed to discriminate these ions from each other. CAPS can also measure ion species which are very difficult to distinguish from each other. For example N_2^+ ions can be distinguish from CO^+ ions although their charges are the same and also masses are very close to each other with mass numbers of about 14 amu each. Also O^+ and CH_4^+ constitute such an isomeric ion pair, which can be distinguished from each other. In order to separate minor ion species the integration period will be increased from 32s to 256s. For more common ions the integration period of 32s is expected to be sufficient.

The CAPS instrument is made up of three complementary plasma sensors: Ion Mass Spectrometer (IMS), Electron Spectrometer (ELS), and Ion Beam Spectrometer (IBS). The location of each of these sensors in the CAPS instrument can be seen in cross-section of CAPS shown in Figure 2.5. IMS consists of a top hat electrostatic analyser followed by a linear electric field time-of-flight analyser. It is designed for studies of the composition and general ion plasma dynamics. ELS is a top hat electrostatic analyser. IBS consists of a hemispherical electrostatic analyser, and is specially designed for studies of ion beam distributions. The field-of-views (FOV) of the three sensors are coplanar. All three sensors are mounted on top of a single data processing unit (DPU) that provides a mechanical interface to

the actuator (ACT). DPU also provides housing for low voltage power, command and control electronics, and spacecraft interfaces. ACT provides a mechanical interface to FPP (see fig. 2.4 for the location of the CAPS instrument aboard Cassini). Due to the rotation capability provided by ACT the CAPS sensors can scan 46% of the sky every three minutes. The spacecraft itself will rotate around its z-axis (see Figure 2.4) with a period of 23 minutes. This, together with the pendulum motion of ACT, increases the CAPS coverage to 83% of the sky over a period of 12 minutes [*Young et al.*, 1996]. The location of the High Voltage Units (HVU) of IMS is marked on Figure 2.5. Due to complexity of the IMS sensor the supporting electronics such as the HVU are located apart from the sensor itself. In the other two CAPS sensors the supporting electronics are placed inside the sensors.

During the development and test phases of the CAPS instrument the functions of the spacecraft were simulated using the Electrical Ground Support Equipment (EGSE). The same EGSE with the engineering model of the CAPS will be used to verify the operations of the CAPS flight model if some problems arise during the mission. EGSE together with the engineering model will be used also when the software upgrades of the CAPS instrument are tested. Thus possible errors can be corrected before they may endanger the reliable functioning of the instrument.

Each sensor or detector of the CAPS is described by a geometric factor defined as follows:

$$G = A \left\langle \Delta\beta \frac{\Delta E}{E} \right\rangle \int_{\Delta\alpha} \cos\alpha d\alpha, \tag{2.1}$$

where

$$\left\langle \Delta\beta \frac{\Delta E}{E} \right\rangle \int_{\Delta\alpha} \cos\alpha d\alpha = \frac{\sum\limits_{ijk} C_{ijk} \delta E_i \delta\beta_j \delta\alpha_k \cos\alpha}{\max\left(C_{ijk}\right)}. \tag{2.2}$$

In Eq. (2.1), A is the area of the entrance aperture. The integration given in Eq. (2.2) implies an integration over the response function in the two angles and in relative energy. In the discrete sum, where the response function is integrated over energy and azimuthal and polar angles, C_{ijk} gives the counts for each ion beam position, δE_i gives the bin width in energy, $\delta\beta_j$ in azimuthal angle and $\delta\alpha_k$ in polar angle. When the geometric factor is calculated using formulas (2.1) and (2.2) the detector efficiency is assumed to be 100%. Using this definition also the laboratory calibration data is renormalized to 100% detector efficiency. Therefore this method does not take the detector efficiency into account, but it only describes the analyser part of the detector. This method is used in Paper III, since it gives an opportunity to compare simulations and calibrations. In the laboratory calibrations the denominator of Eq. 2.2 is often replaced by the beam monitor count number. In this case the detector efficiency ξ is included in the geometric factor. Often the aperture area A in Eq. 2.1 is also replaced by the effective area A_{eff}:

$$A_{eff} = A\xi. \tag{2.3}$$

The geometric factor which includes all the effects mentioned above is also called sensitivity.

2.4.2.2. Ion Mass Spectrometer (IMS)

IMS is the most complex of the three spectrometers of the CAPS instrument. It is an isochronous time-of-flight (TOF) mass spectrograph with unique features that address the need for both high sensitivity and high resolution mass analysis in a single instrument. It has the capability to measure ions from 1 to 50000 eV/q energies with a 17% energy ($\Delta E/E$) resolution. (q is the ion charge). The mass range is 1 to 60 amu/q, and the mass resolution ($M/\Delta M$) is 80 for ions with energies less than 16 keV/q, and 8 for ions with energies more than 16 keV/q. The FOV range is $11^\circ \times 160^\circ$ which consists of eight separate sectors with separate detectors, each providing an angular resolution of $11^\circ \times 20^\circ$. The time resolution of IMS is 62.5ms for a single sample, and 4s for the whole angle/energy/mass spectrum. The sensitivity for total FOV is 10^{-3} and for pixel FOV 10^{-4} when $M/\Delta M$ is 80, and when $M/\Delta M$ is 8 the sensitivity for total FOV is 10^{-2} and for pixel FOV 10^{-3}. The unit of sensitivity is $cm^2 sr(eV/eV)(counts/particle)$ [*Young et al.*, 1996].

The basic operation principle of the IMS sensor is quite simple (See Fig. 2.6). First the ions enter the top hat electrostatic analyser (ESA) which passes through the ions with a specific energy per charge E/q ($=k_{ESA}$) ratio. The toroidal top hat electrostatic analyser is described in more detail in *Young et al.* [1988]. After that the ions are accelerated using 15 kV voltage. Thus the total ion energy, before entering to the Linear Electric Field (LEF) area, can be written

$$E_{tot} = k_{ESA} q + 15keV, \tag{2.4}$$

where k_{ESA} is a constant which defines the ion motion at ESA. After that the ions collide and pass through the thin carbon foils providing secondary electrons which enter the LEF area, where the electrons are accelerated before they strike Micro Channel Plates (MCP) located at the bottom of IMS (see Figures 2.6 and 2.7). Thus the starting pulse of the TOF measurement is created in the MCPs using secondary electrons from the carbon foils. Simultaneously the ions continue their flight, and the LEF decelerates the ions so that they return to MCPs located at the top of the LEF area, producing the stop signal of the TOF measurement. In this case the LEF area is an isochronous TOF analyser with high mass resolution ($M/\Delta M \approx 80$). Since the electric field is linear the force F at the LEF area can be written as

$$F = -q k_{LEF} x. \tag{2.5}$$

The constant k_{LEF} is determined via the linear electric field at LEF. When the equation of motion of the ion is now solved it can be seen that the result is ordinary harmonic equation

$$x = h \sin\left(\sqrt{\frac{q k_{LEF}}{m}} t\right). \tag{2.6}$$

The coordinate system used in the equations 2.5 and 2.6 is defined in Figure 2.8. Using the periodicity of the equation 2.6, it can be seen that the flight time t_{ft} of

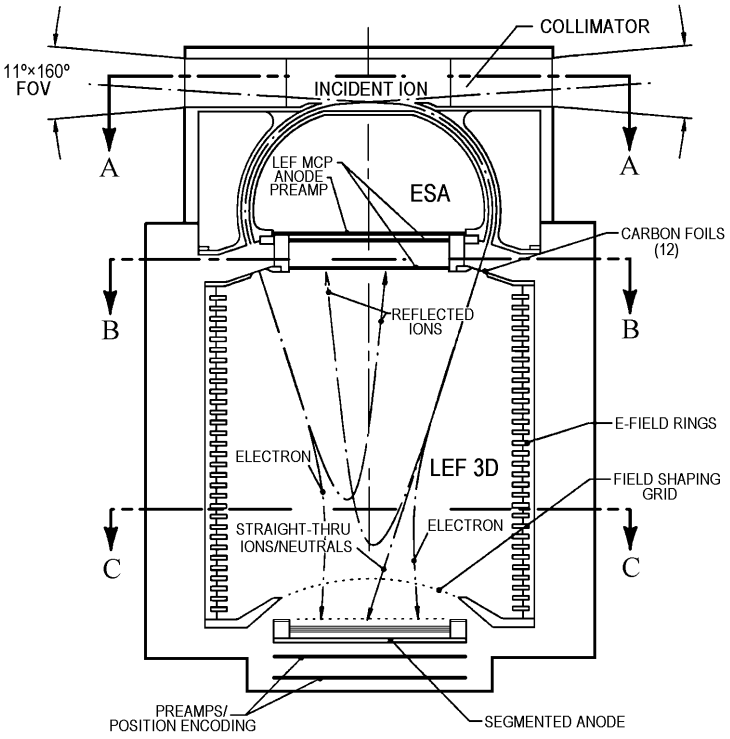

Fig. 2.6. Cross-sectional side view of IMS. IMS FOV is marked on the figure. The top hat ESA is on the top of the figure, and LEF is located below it. The Micro Channel Plates (MCP) are used to detect ions after the LEF area. The cross-sections A-A, B-B and C-C refer to Figure 2.7, where the top view of IMS is presented (from *Young and Jensen* **[1993]).**

the ion is

$$t_{ft} = \frac{\pi}{\sqrt{\frac{qk_{LEF}}{m}}}. \tag{2.7}$$

When k_{LEF} is known and t_{ft} measured accurately the relation m/q will be determined unambiguously. If the ions have enough energy, so that the LEF has not enough force to turn them, they will continue to the MCPs at the bottom of the LEF area, and produce the stop signal of the TOF measurement there. In this case the mass resolution ($M/\Delta M$) is 8.

Although the very basic idea of IMS is relatively simple the instrument itself is quite complex. In the description given above only single ion nuclei are considered. IMS can also detect more complex, molecular ions. In that case the ESA part works as before but the molecular ion breaks down at the carbon foils producing the starting signal and ions and neutral nuclei which arrive in the LEF area. Now,

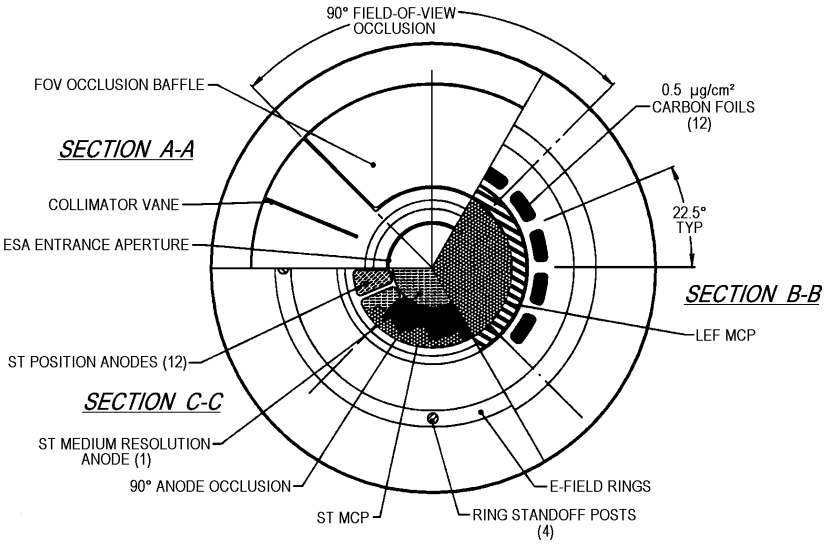

Fig. 2.7. Top view of IMS. Section A-A shows ESA, section B-B shows the part between ESA and the LEF area, and section C-C shows the lower part of LEF as demonstrated in Fig. 2.6. The parts in the C-C-section which are used to produce the starting signal of the TOF measurements from the secondary electrons are marked as ST (from *Young and Jensen* **[1993]).**

ion nuclei behave in the LEF area as described in the previous paragraph, but the neutrals continue directly on to the MCPs located at the bottom of the LEF area. Thus, all particles produced in the carbon foils from original ions can be detected. This provides the very high measurement efficiency of the IMS sensor. Each separate part of the original complex ion will produce its own stop signal for the TOF measurement, and the collected data of the single complex ion will increase notably. In the Spectrum Analyser Module (SAM) of DPU the data can be analysed in detail and the properties of the original complex ion can be traced [*Sittler*, 1993]. Using this method IMS can separate isomeric ions such as N_2^+ and CO^+ which normally require a mass resolution ($M/\Delta M$) of 2800. Naturally the complexity of the IMS requires very careful calibrations so that the complex data set produced by IMS can be properly analysed. More details about the IMS can be found in [*McComas and Nordholt*, 1990; *McComas et al.*, 1998; *Nordholt et al.*, 1998; *Young et al.*, 2003].

The IMS assembly in CAPS is shown in Figure 2.5. IMS is also a basement for the ELS instrument and provides enough space between the FOV of the ELS and CAPS surfaces so that the sensitive electron plasma measurements will not be disturbed by the secondary electrons emitted from the CAPS surface.

The physical dimensions of IMS are shown in figure 2.8. During the launch

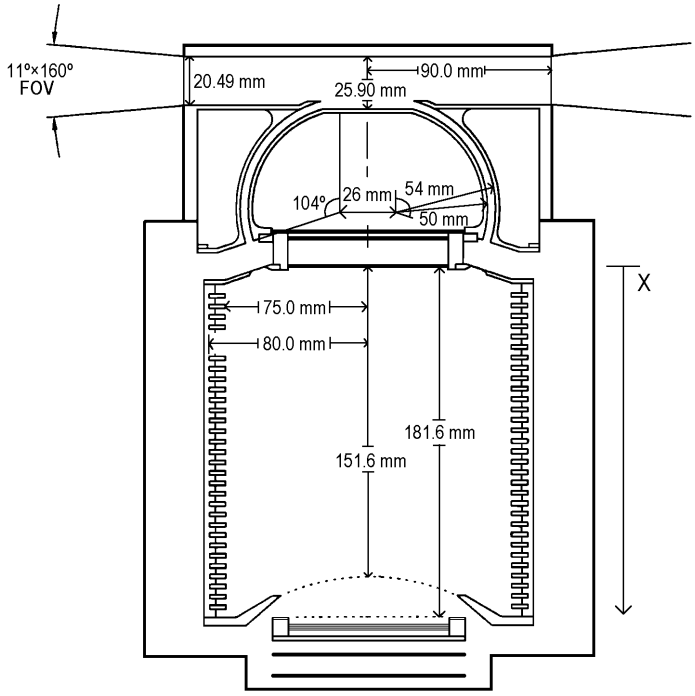

Fig. 2.8. The physical dimensions of the IMS instrument. (The figure is modified from *Young and Jensen* **[1993].)**

the entrance aperture was covered so that the carbon foils inside the IMS did not contaminate and did not suffer acoustic damage. The covers were released using a thermal wax actuator. The LEF cylinder is surrounded by 30 metallic rings which are supplied with voltage, and thus produce the linear electric field of the LEF area. The dimensions of IMS were selected after detailed studies of ion trajectories inside the IMS instrument using ray tracing and analytical orbit calculations.

2.4.2.3. Electron Spectrometer (ELS)

The Electron Spectrometer (ELS) is exclusively planned for electron measurements. The analyser of ELS is a typical top hat electrostatic analyser commonly used in space plasma instrumentation. Electrons enter through an entrance aperture which is divided into 8 sectors. The spherical electric field bends the electron paths and only those electrons with a specific energy per charge (E/q) ratio can

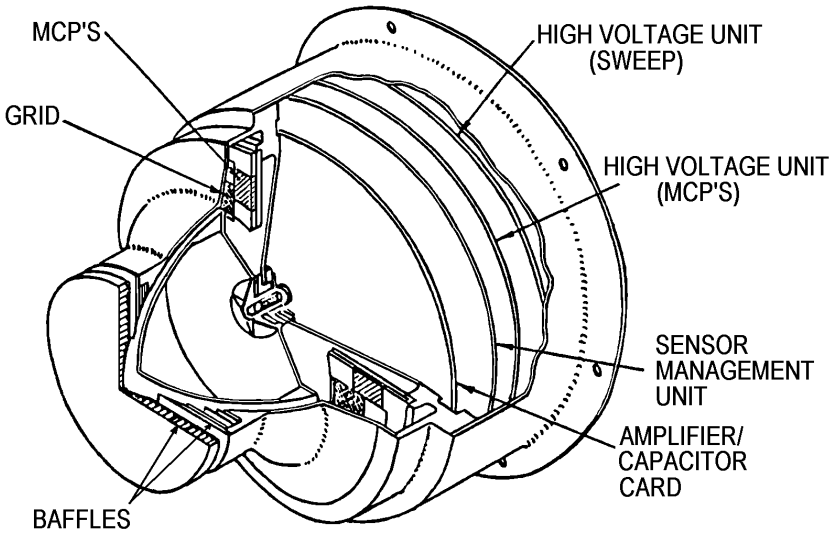

Fig. 2.9. The Electron Spectrometer. The top hat electrostatic analyser is on the left, and the supporting electronics on the right. Also the micro channel plates are marked in the figure (from *Young and Jensen* **[1993]).**

pass the analyser. The transmitted electrons collide with the eight MCPs, and appropriate counting signals are produced. Thus the ELS data yields information on the number of electrons per energy/charge per angle. ELS provides 17% energy ($\Delta E/E$) resolution for electrons from 0.6 to 27 keV energies. The angular range of ELS is $5°\times160°$, consisting of eight sectors with separate detectors, each of which providing $5°\times20°$ angular resolution. The time resolution for a single sample is 31.25 ms, and 2 s for the whole energy/angle spectra. The sensitivity for the total FOV is 10^{-2} and for pixel FOV 10^{-3} $cm^2sr(eV/eV)(counts/particle)$. The geometric factor of single 20° anode is 1.7×10^{-3} cm^{2}sr, for total field of view it is 1.4×10^{-2} cm^{2}sr.

The cross-sectional view of ELS is presented in Figure 2.9. The coaxial mounting of ELS and IMS is clearly visible in Figure 2.5. The supporting electronics of the ELS sensor is placed at the bottom of the instrument. Thus the location of the sensor is such that the FOV of the instrument is optimal. This guarantees that CAPS does not obscure the FOV of ELS. (Note that despite precautions the ELS and IMS FOV's are obscured by the frame of the Cassini spacecraft. The obscured sector is marked also in Figure 2.7, where the IMS top view is presented.) This lay-out also prevents the scattered or secondary electrons from the CAPS surface from entering the analyser.

The construction of the ELS instrument is typical for a top hat electrostatic analyser, which turns the electron paths approximately 90°. Actually there is a

15.0° deficiency at the bottom of the hemispheres, and the turn angle is rather 75.0° than 90°. The outer radius of the inner hemisphere is 40.0 mm and the inner radius of outer hemisphere is 43.0 mm at the lower parts of the hemisphere and 46.4 mm at the top of the hemisphere, where the electron entrance aperture is located. Thus the gap between the hemispheres (ΔR) in the lower part is 3.0 mm. The dimensions of the entrance aperture of the collimator are such that each of the eight 20° subsectors is 1.53 mm wide. These dimensions lead to resolutions and sensitivities given in the previous paragraphs [*Young and Jensen*, 1993]. A detailed description of ELS can be found in *Coates et al.* [1992], *Linder et al.* [1998] and *Young et al.* [2003].

2.4.2.4. Ion Beam Spectrometer (IBS)

The third plasma sensor of CAPS is the Ion Beam Spectrometer (IBS) which is a single hemispherical electrostatic analyser with three fan-shaped entrance windows for incoming charged particles (see Fig. 2.10). Channel electron multipliers (CEM) are used as detectors in the IBS instrument [*McComas and Bame*, 1984; *McComas et al.*, 1987]. Ions enter the instrument through three entrance apertures into the spherical electric field applied between the hemispheres of IBS. Only ions with a specific energy per charge (E/q) ratio can pass through the electrostatic analyser and collide with the carbon foils of the CEMs. The collision of each single ion produces secondary electrons which are accelerated inside CEM to produce the counted signal. During the secondary electron event CEM is insensitive to new ion collisions at the carbon foils, and thus an appropriate dead time correction has to be applied to the total counting rates. Thus the IBS data yields the information on transmitted ions per aperture per a specific energy channel.

IBS has a 1.5 % energy resolution ($\Delta E/E$) for ions with E/q from 1 to 50000 eV/q. The angular range for each entrance windows is 1.5°×150°. When data from all entrance windows is analysed together, the angular resolution is at its best 1.5°×1.5°. This resolution requires the usage of the higher bit rate data modes when all angular resolution is still in the data, and the crossed fan analysis with best angular resolution with at least two fans.

The time resolution of IBS is 7.8125 ms for a single sample and 0.5 s for an entire energy/angle spectrum. The sensitivity is 3×10^{-5} for total FOV and 10^{-6} for single pixel FOV. The high angular and energy resolutions of IBS enhance the capability of CAPS to measure highly directional plasma flows. This includes solar wind plasma flow, and the narrow field-aligned currents in auroral regions, as well as highly rammed dense plasma in Titan's ionosphere during Titan flybys [*Young et al.*, 2003]. Thus a remarkable addition to the information on ion plasma is obtained. More about the response function, energy, and angular resolution of IBS is presented in Papers I–III, where the IBS simulations and calibrations are considered in detail.

The top view of the IBS spectrometer is shown in Figure 2.10/A and the side view in Figure 2.10/B. The supporting electronics of the IBS sensor is located inside

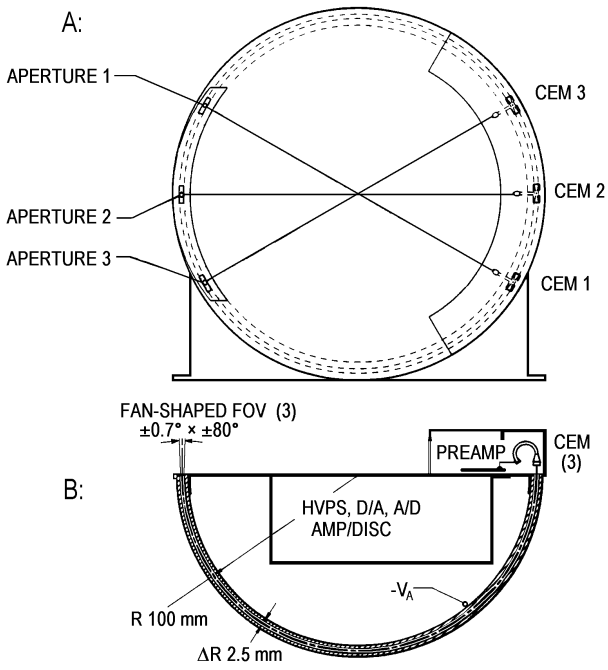

Fig. 2.10. **A. Top view of IBS. B. Side view of IBS. Three apertures and corresponding three CEM particle counters are marked on the figure. The cross-section is similar for all aperture/CEM detector pairs. The supporting electronics, like high voltage units (HVPS) and D/A and A/D converters, are located inside the hemispheres. The side view of CEM is shown in B. The dimensions of IBS are also marked on the figure (from** *Young and Jensen* **[1993]).**

the hemisphere of the instrument. The plate thickness of the hemispheres is 0.50 mm. The outer radius of the inner hemisphere is 98.75 mm and the inner radius of outer hemisphere 101.25 mm. Thus the gap between the hemispheres (ΔR) is 2.5 mm, mid-radius (R) is 100.00 mm, and their ratio ($R/\Delta R$) is 40. Actually, IBS is not exactly hemispherical, since the angle from the apertures to the CEMs is only 178°. The angle between the midpoints of adjoining entrance apertures is 30°. The dimension of the apertures is 15.0×2.5mm. A detailed presentation of the IBS mechanics and geometry is given in *Young and Jensen* [1993] and *Hannula* [1994]. The IBS hemispheres were manufactured at VTT Automation in Otaniemi, Espoo, Finland. University of Oulu has also participated in the development of the IBS instrument. The simulations were planned and coded in Oulu. Oulu has also participated in the calibration data analysis.

2.4.2.5. Data Processing Unit (DPU)

The CAPS data is preprocessed in the Cassini spacecraft using the Data Processing Unit (DPU). DPU transmits the processed observations to the spacecraft computers which then transmit the data to Earth using the high-gain antenna (HGA). DPU also controls the actuator. DPU consists of three PACE 1750A microprocessors operating 1.2 MIPS at 20 MHz. Their speeds correspond approximately to that of Intel 80386 processor. However, in CAPS they are operated at a lower rate. Two of the processors operate as normal Central Processing Units (CPU) and one as a spectrum analyser in Spectrum Analyser Module (SAM). The memory capacity of DPU is such that both DPU CPUs together have 448 kwords RAM and a 64 kwords ROM. ROM has a software required to boot the DPU. The RAM memory can be used to store data or to contain program codes. During the booting of DPU the software will be loaded to RAM from the spacecraft solid state recorder or directly from the ground. Thus, the CAPS software can be updated during the mission, and new measurement modes can be added if some specific study requires it [*Young et al.*, 1996].

One of the CPUs controls the operation and data processing of the simpler ELS and IBS sensors. It also controls IMS operations. The other CPU is fully dedicated to the IMS data analysis and compression. Due to its complexity, the IMS has a special role in the data processing. SAM is designed to preanalyse and compress the data collected by IMS. SAM will operate as a DPU slave, and therefore it has no direct access to the memory of DPU. The very complex information of an ion event described in detail in section 2.4.2.2 will be analysed and combined. This requires a complex data compression [*Young et al.*, 1996].

2.4.2.6. Actuator (ACT)

The actuator (ACT) provides a rotation capability for the CAPS instrument using a stepping motor [*Ylikorpi and Luntama*, 1995; *Young et al.*, 1996, 2003]. It allows for a $\pm 104°$ rotation, of which $184°$ at angular speed of $1°/s$. The remaining two $12°$ sectors at the both end of the scan range are used to change the direction of rotation of the CAPS, which means the deceleration before and acceleration after the turning point of the CAPS. Angular measurement accuracy is $\pm 0.5°$. The mechanics of ACT limits the rotation to $\pm 110°$. ACT provides also the mechanical interface for the CAPS instrument to the fields and particles pallet of the Cassini spacecraft. Because ACT had to carry the mass of CAPS ($\sim$18kg) during the launch, a specific latch ring assembly was used to prevent the ACT to move. After eight days of flight the latch was successfully released using a wax thermal actuator. VTT Automation from Otaniemi, Espoo has manufactured the actuator, and Rejlers OY was involved in the development of the ACT.

2.4.3. Simulations of the Ion Beam Spectrometer

High resolution spherical electrostatic analysers have commonly been used in space plasma physics research. The very high (∼1 %) energy resolution of the IBS requires a high precision in both fabrication and in the alignment process. The simulations were developed using the Monte Carlo method. In Paper I, random distributions for energy and angles were constructed and the analyser acceptance were calculated using the ray tracing method. In other words the ions which collide with the analyser plates were rejected and ions which transmitted the analyser were accepted. All ions in Paper I were injected from a narrow slit at the middle of the analyser aperture. This was reasonable since the effect of different errors in the analyser acceptance was studied. The goal of the simulations was to calculate the upper limits of the geometrical tolerances of the IBS instrument for which fixed baseline dimensions and specifications had been given. The simulation model were used to check whether the available manufacturing technology were adequate or not. In other words, the manufacturing costs were optimized. Paper I presents a calculation method that describes the performance of the IBS instrument and how the influence of the geometrical manufacturing and assembly errors can be estimated. In particular, the misalignment of the hemispheres has been considered with special care. Also the influences of indentations on the surfaces of the hemispheres was considered. The energy resolution of observed ions has been estimated to be $\Delta E/E = (1.6 \pm 0.2)$ %, and the maximum loss of transited particles with respect to the transmission of an ideal instrument has been defined as 10 %. Similarly it has been specified that the deviations in the distributions of entrance angles of transited particles are less than 0.1 degree. As a result, the 25 μm specification was given to all geometrical manufacturing errors although only the misalignment was studied by simulations directly.

It was found that indentations up to a depth of 300 μm and over an appreciable area did not affect significantly the transmission properties of the IBS instrument. Fortunately, the size of indentations or elevations expected in manufacturing is typically much smaller than that used in calculations presented in Paper I. In practice the 300 μm indentation depth should be considered quite large since even a depth of 100 μm can easily be mechanically detected. Therefore, a nominal upper limit of 100 μm for an indentation was chosen. The assembly tolerance of the hemispheres has been confirmed to be of the same order of magnitude. The hemispheres were measured mechanically by using a touch sensor which yields a 5μm accuracy.

In Paper II IBS is considered more realistically as a hemispherical electrostatic analyser equipped with an aperture plate to improve the collimation of the stray electric field at the entrance apertures. The influence of a curved entrance aperture has also been included in the simulation model, and its effects have been studied in detail. The stray electric field was calculated using a cylindrical (3D) simultaneous over-relaxation (SOR) algorithm [*Press et al.*, 1986]. In practice this gave an opportunity to study the butterfly effect considered by *Gosling et al.* [1978, 1984]. The model in Paper II introduced the simulation of the laboratory ion beam. The ions were injected with an evenly distributed random energy for the narrow

laboratory ion beam. The ion trajectories were then calculated, and each ion which did not collide with the front aperture plate or analyser plate was accepted. Ion trajectories inside the IBS instrument were calculated using the method described in Paper I. Basically the aim was to simulate the function of the IBS instrument as realistically as possible in distinction to Paper I where the only interest was in the properties of the hemispheres. As a result, the energy resolution of the IBS instrument improved from $\Delta E/E = (1.6 \pm 0.2)\%$ given in Paper I to $\Delta E/E = (1.3 \pm 0.2)\%$. The improvement was due to the front aperture plate cutting off some ion trajectories with very low or very high relative energies, and also to the collimating effect of the stray electric field on the ion beam. Because of the butterfly effect the azimuthal angle resolution changed from the idealistic value $\beta = (1.4 \pm 0.1)^\circ$ given in Paper I to the more realistic $\beta = (2.3 \pm 0.1)^\circ$. In Paper II it was also proved that the manufacturing accuracy of 25μm of the IBS instrument given in Paper I was still sufficient. It was also demonstrated that the deviation in the energy distribution is less than 0.2% and that the deviation in the entrance angle distribution of of transmitted particles is less than 0.1° also when the entrance aperture is included in the simulations.

In Paper III the response function of a hemispherical electrostatic analyser equipped with a curved aperture plate was calculated. The simulation algorithm differs from the algorithm given in Papers I and II in several aspects. The calibration results of the IBS flight model show an unexpected double curved shape in the energy/polar angle distribution. A new asymmetric geometry for the inner hemisphere was introduced and simulated. Otherwise the simulation concept was similar to the one in Paper II. Using the new simulation model the calibration results were better understood. When the simulation and laboratory calibration results were combined, the energy resolution of the IBS flight model was found to be $(2.0 \pm 0.1)\%$ (FWHM value), the angular resolution was $(3.1 \pm 0.1)^\circ$ (FWHM value), and finally the geometric factor was $(2.5 \pm 0.1) \times 10^{-4}$ cm^{2}sr. The notable difference in energy resolution when comparing results of Paper I and II to results of Paper III is mainly because of the double curved shape of the energy/polar angle distribution. When the polar angle is integrated over such a distribution, a wider energy distribution is produced than in a straight distribution of Paper I and II.

3. Wavelet technique

We have used the wavelet transformation technique when producing dynamic power spectra in order to find the possible quasi-periodicities in the different data sets like geomagnetic activity (Paper IV), solar wind velocity (Papers IV and V) and magnetic field intensity (Paper V). The wavelet transformation was chosen because it gives an optimal resolution between time and frequency domains. Moreover, it gives the possibility to increase or decrease the resolution in one domain with respect to the other. More conventional methods like Fourier transformation and maximum entropy methods give the best possible frequency resolution, but the time resolution in these methods is always limited to selected time interval. Very similar results compared to wavelet transformation can be obtained using for example the band pass convolution filter technique. (Compare Paper IV using the wavelet technique, and *Mursula and Zieger* [2000] using the convolution filter technique.) Wavelet transformation was calculated using the complex Morlet wavelet [*Holter*, 1995; *Lagoutte et al.*, 1992]. The Morlet mother wavelet $g(t)$ is defined as

$$g(t) = e^{i\omega_0 t} e^{-\left(t^2/(2\sigma^2)\right)}, \tag{3.1}$$

whence its Fourier transformation $G(\omega)$ becomes as follows

$$G(\omega) = \sqrt{2\pi}\sigma e^{-\sigma^2(\omega-\omega_0)^2/2}. \tag{3.2}$$

Thus the Morlet wavelet consists of cosine and sine oscillations with a Gaussian window as its real and imaginary parts. In Eqs. 3.1 and 3.2 t is time, i denotes the imaginary unit, ω_0 is basic angular frequency of the wavelet, σ parameter defines the width of the windowing Gaussian function, and the ω is angular frequency. For the classical Morlet wavelet $\omega_0 = 5.34$ and $\sigma = 1$.

Two Morlet mother wavelets, one with $\omega_0 = 5.34$ and $\sigma = 1$, and the other with $\omega_0 = 5.34$ and $\sigma = 2$ are depicted in Figure 3.1 together with the corresponding Fourier transforms. As can be seen in Eq. 3.2 one can change the frequency resolution of the wavelet transformation by changing the value of the parameter σ. (Another choice would be to modify the parameter ω_0, but in Papers IV and V we have changed the σ parameter.) When σ is changed from 1 to 2 or further

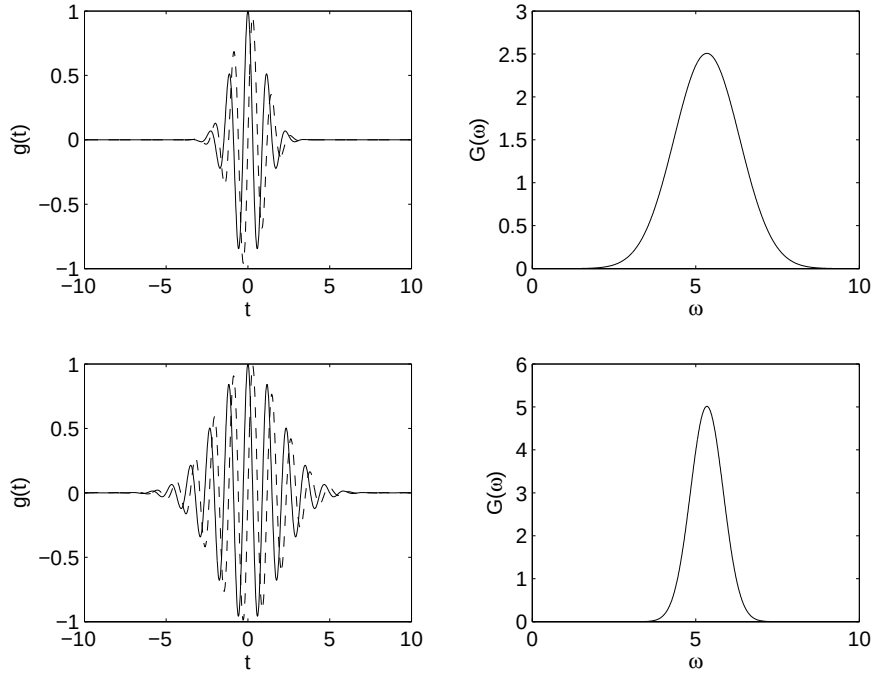

Fig. 3.1. **Classical Morlet mother wavelet ($\omega_0 = 5.34$) and its Fourier transformation in two cases: above for $\sigma = 1$; below for $\sigma = 2$. The solid line (and dashed line) gives the real (imaginary) part of the mother wavelets.**

to 4, the width of the Gaussian window is increased. The frequency resolution (corresponding to power decrease to one half; 3 dB in amplitude) is $\pm 15.6\%$ for $\sigma = 1$, $\pm 7.8\%$ for $\sigma = 2$, and $\pm 3.9\%$ for $\sigma = 4$. Thus by doubling the σ parameter we also double the frequency resolution. However when the frequency resolution is increased the time resolution is decreased. The time resolution at period T is 1.42 T, 2.83 T, and 5.68 T for $\sigma = 1$, 2 and 4, respectively. Actually when we pick a very high value for the σ parameter we approach the traditional Fourier transformation, which loses the time resolution completely and has the highest possible frequency resolution. When we study very long time series, like geomagnetic activity in Paper IV, we have to use also higher σ parameter values than 1. In fact, for all parameters studied in Papers IV and V we have prepared different wavelet spectra using at least 2 (and often more) σ values. Note also that a higher σ value means that the cone of influence at the edges of the wavelet transformation is increased. Therefore very high σ values are useless in short data sets. Note also that the cone of influence effect can be reduced by subtracting the average of the studied signal before processing it through the wavelet algorithm.

After selecting the mother wavelet we can calculate the wavelet transforma-

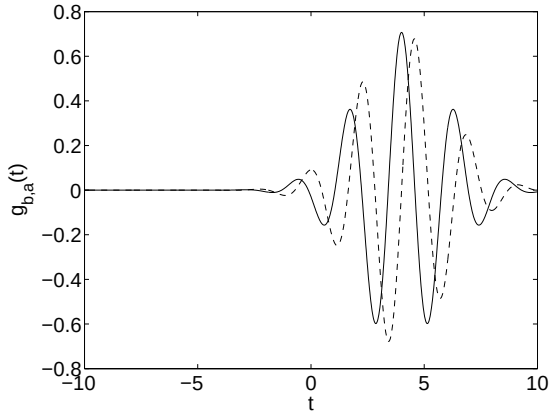

Fig. 3.2. Effect of scaling (a = 2) and translation (b = 4) on the classical Morlet wavelet ($\omega_0 = 5.34$ and $\sigma = 1$). The solid line (and dashed line) gives the real (imaginary) part of the wavelet.

tion. In the wavelet transformation we repeatedly scale and translate the mother wavelet. The definition for the scaled wavelet $g_{b,a}$ is

$$g_{b,a} = \frac{1}{\sqrt{a}} g\left(\frac{t-b}{a}\right) \qquad b \in \Re, a > 0, \tag{3.3}$$

where the a parameter defines the scale and b parameter the translation. The normalization factor $1/\sqrt{a}$ ensures that the energy is conserved between transformations at different scales. In Figure 3.2 we have demonstrated how scaling and translation change the classical Mother wavelet ($\omega_0 = 5.34$ and $\sigma = 1$) depicted in the upper panel of Figure 3.1.

The wavelet transformation $C(b, a)$ is then defined as a convolution integral of the studied signal $x(t)$ and the scaled and translated wavelet $g_{b,a}$:

$$C(b,a) = \sqrt{2} \int x(t) g^*_{b,a}(t) dt \qquad \omega \in [0, +\infty] \tag{3.4}$$

$$C(b,a) = 0 \qquad \omega \in [-\infty, 0[. \tag{3.5}$$

The physical analysis is usually done in the time-frequency plane instead of the given time-scale plane. Therefore, a transformation to the more physical variables has to be made by rescaling the frequency f as follows:

$$f = \frac{f_0}{a}, \tag{3.6}$$

where $f_0 = 0.85$ $(= \omega_0/(2\pi))$ is the frequency of classical Morlet mother wavelet.

The wavelet transformation is then

$$H\left(b, \frac{f_0}{f}\right) = \frac{1}{\sqrt{K_g f_0}} C\left(b, \frac{f_0}{f}\right), \tag{3.7}$$

where

$$K_g = \int_0^{+\infty} |G(\omega)|^2 \frac{d\omega}{\omega}, \tag{3.8}$$

is constant and depends only on the analysing wavelet. The last step is then to discretize the formula 3.7, and calculate the convolution numerically. The modulus squared of the wavelet amplitude gives the power of the signal which can then depicted as a dynamic spectrum. More details about the method are given e.g. in *Lagoutte et al.* [1992], *Torrence and Compo* [1998] and *Holter* [1995].

4. Mid-term quasi periodicities

Here we discuss the so called mid-term quasi periodicities (MTQP) which have been defined to cover the periodicity range from one year to two years. Oscillations in the MTQP range have been observed in several parameters in the Sun and in the heliosphere. The recent increase of interest in MTQP related phenomena started when *Richardson et al.* [1994] reported a new strong 1.3-year periodicity in solar wind speed observed in IMP-8 and Voyager 2 from 1987 to 1993. This is the most intense MTQP event in solar wind speed according to our analysis in Paper IV, and has been verified by several other observations in the different parts of the heliosphere, as discussed in Paper V. Soon after the finding by *Richardson et al.* it was reported that a 1.3-year periodicity exists also in the geomagnetic ap index simultaneously with the solar wind speed [*Paularena et al.*, 1995]. Since long-term geomagnetic activity is closely related to solar wind properties, as discussed earlier in section 1.4, this connection was not a surprise. *Gazis et al.* [1995] used a number of heliospheric probes to show that the 1.3-year periodicity is a global phenomenon in the heliosphere from 0.7 AU to 60 AU. *Gazis* [1996a] also proved that these solar wind enhancements resemble more the changes over the sunspot cycle rather than the shorter term fluctuations due to, e.g., coronal mass ejections or interaction regions. This observation suggested that the 1.3-year fluctuations in the heliosphere are of solar origin and do not arise, e.g., from the migration of of perturbances during heliospheric propagation.

The long-term persistence of MTQP oscillations has been demonstrated even earlier by a peak at 1.4 years in the power spectrum of the occurrence of visual aurora in Sweden from 1721 to 1943, as reported by *Silverman and Shapiro* [1983]. More recently, it was found by *Howe et al.* [2000] using helioseismological measurements that the rotation speed at the bottom of the solar convection layer is fluctuated at the 1.3-year periodicity. This suggests that the solar dynamo, which is expected to be located in this region, and thereby the magnetic flux that it generates is modulated at this periodicity. *Ichimoto et al.* [1985] studied Hα flares and found a 17-month (1.4-year) periodicity during solar cycle 21 both in the northern and southern hemisphere. They also noted that these fluctuations in the two hemispheres are in anticorrelation. *Akioka et al.* [1987] reported that the same periodicity exists simultaneously also in sunspot activity. Even earlier

Yacob and Bhargava [1968] mentioned a 16-month (1.3-year) periodicity in Wolf sunspots numbers and in the quiet-day range of the geomagnetic horizontal force at the Huancayo station. *Yacob and Bhargava* [1968] studied the time interval from 1905 to 1965. The sunspot data has also been analyzed in *Krivova and Solanki* [2002] using the wavelet transformation method. They find evidence of a 1.3-year periodicity from 1930 to 1955, when, at the same time, we found in Paper IV MTQP oscillations in geomagnetic activity. However *Krivova and Solanki* [2002] do not find activity in 1.3-year periodicity during solar cycle 22, when solar wind speed has its highest fluctuations. *Krivova and Solanki* [2002] also suggest that the 1.3-year periodicity could be the 3rd harmonic of the 150-160 day periodicity first found by *Rieger et al.* [1984] in solar flares.

When considering the longer period range of MTQP fluctuations *Belmont et al.* [1966] found a 19-month (1.6-year) periodicity in 10.7-cm solar radio flux between 1947 and 1964 (solar cycles 18 and 19). A very important finding was made by *McIntosh et al.* [1992] who, when studying the long-term coronal hole development, found a 600-day (1.65-year) periodicity in the coronal hole area of the southern solar hemisphere during the 21st solar cycle. Also our findings in Paper V show that the 1.7 year periodicity was stronger in the southern hemisphere at this time. *Özgüç and Ataç* [1989] have reported a 18.5-month (1.54-year) periodicity in flare index during solar cycle 20 and 21. A 1.68-year periodicity was found in simultaneous measurements of cosmic rays by *Valdes-Galicia et al.* [1996]. The same periodicity is also found in the solar wind speed at 1 AU and in the geomagnetic activity *Mursula and Zieger* [2000]. Also our results in Paper IV and Paper V support this. A periodicity of about 1.8 years has been recently reported by *Kato et al.* [2001] in cosmic ray measurements of Voyager 1 and 2 during the negative polarity of the solar magnetic field (1982-1990). During the positive polarity period this periodicity vanished.

Paper IV gives so far the longest estimation of MTQP oscillations in the solar wind speed using the long-term measurement of geomagnetic activity. Using this estimation we have shown that the long-term MTQP activity roughly follows the long-term solar activity. This is true for the high MTQP power during the high solar activity times in mid-19th century and during the last 70 years, and for the low MTQP power during the weak solar activity around 1900. When discussing the details of this connection in Paper IV we also noted that the MTQP power already decreased during solar cycle 11 which is the last high activity cycle before the long sequence of low activity cycles 12-16. Therefore we suggested that, taking into account the connection of MTQP oscillations and the solar dynamo, a possible decrease in the MTQP range power could indicate the forthcoming long-term decrease of solar activity. The above results were based on the correction in Paper IV of the normalization method used in *Lockwood* [2001]. It has been found [*Mursula and Zieger*, 1999, 2000] that the dominant MTQP period in geomagnetic activity (and solar wind speed at 1 AU) oscillates from a shorter period of about 1.2-1.4 years and a longer period of about 1.5-1.8 years. This alternation persists since 1930s covering the solar cycles from 16 to 22. We have verified this alternation in Paper IV, and show further that it is present even in the mid-19th century.

In Paper V we have the opportunity to use all solar wind and IMF data measured

in the outer heliosphere by Pioneer 10 and 11 and Voyager 1 and 2 probes to study MTQP fluctuations. We have also used OMNI database to give a reference at 1 AU to the study in the outer heliosphere. We have verified several earlier findings and found many new aspects about the MTQP fluctuations using the wavelet technique. As a new result we have, e.g., studied the occurrence of both 1.3-year and 1.7-year fluctuations during solar cycle 22. We have shown that these two periodicities are latitudinally organized. The 1.3 year periodicity, which occurs in solar wind speed is located in the region close to the solar equator. We have suggested that low latitude coronal holes produce this periodicity. The equatorial origin is also supported by the fact that this periodicity is strongest in those probes (1AU OMNI, Pioneer 10, and Voyager 2) that are close to the equator during the event. At higher latitudes like Pioneer 11 no evidence is found for a significant 1.3-year periodicity.

On the other hand, the 1.7-year periodicity occurs at mid-latitudes. However, due the flux tube expansion from high to low latitudes [*Wang and Sheeley*, 1990], this periodicity is detected strongly also in IMF magnitude at 1AU during cycle 22. Thus these observations show that the two different MTQP fluctuations (1.3-year and 1.7-year) coexisted during solar cycle 22 in different parameters. However, only the 1.7-year periodicity was observed during solar cycle 21, indicating differences between the two consecutive solar cycles forming one magnetic cycle. Also, the various parameters depict a hemispherically asymmetric behavior for the 1.7-year fluctuations during cycle 21. In line with the above mentioned observations of hemispherical anticorrelations, we noted in Paper V that the helioseismic studies would not have observed the 1.7 periodicity if they are hemispherically antisymmetric since the method used by *Howe et al.* [2000] can only detect north-south symmetric signals. However, in Paper V we have analyzed data during solar cycle 21 and 22, while *Howe et al.* [2000] analyzed data from 1995 to 2000 (ascending phase of solar cycle 23). Accordingly, temporal changes may also be the reason for the observed differences between the MTQP patterns found in the heliospheric parameters and in the helioseismic observations.

5. Conclusions

In this thesis the properties of a high resolution hemispherical electrostatic analyser, the Ion beam spectrometer (IBS) of the Cassini plasma spectrometer (CAPS), are studied in detail in Papers I–III. IBS is designed to detect narrow ion beams in the Saturnian magnetosphere, and also act as a solar wind monitor. A simulation model has first been used to estimate the requirements in the assembly of the hemispheres. The simulation model has been developed further in order to understand the calibrations of the actual IBS flight model. Thus the simulations have been a remarkable tool when the properties and scientific capabilities of the IBS has been estimated. They have also given important information for the development of the IBS flight software and data analysis methods. Work on the latter topic will continue with the analysis of measured data from the CAPS instruments during the coming years.

The properties of mid-term quasi periodicities (fluctuations with 1-2-year period) have been studied in detail in Papers IV and V. While Paper IV presents the temporally longest study of MTQP fluctuations, Paper V gives the spatially widest treatment of the same phenomenon in the heliosphere. We have studied the appearance of MTQP fluctuations in solar wind speed at 1 AU using the longest available series of geomagnetic activity. It was shown that the long-term occurrence MTQP fluctuations roughly follows the long-term solar activity, suggesting that MTQP fluctuations are closely connected with the solar dynamo activity. Moreover, it was also noted that MTQP activity may offer a possibility for a precursory signal which could be used to predict significant changes in long-term solar activity. We have studied the MTQP fluctuations in solar wind and interplanetary magnetic field measured in the different locations of the outer heliosphere. It is shown that two MTQP fluctuations of different periods (1.3 and 1.7 years) coexisted during solar cycle 22, while during solar cycle 21 only the 1.7-year band existed. This suggests that the solar dynamo acts differently during even and odd cycles. It is also shown that the two MTQP fluctuations during solar cycle 22 are organized latitudinally. While the 1.3-year periodicity originates from equatorial regions, the 1.7-year fluctuations arise at mid-latitudes.

References

Akioka, M., J. Kubota, M. Suzuki, K. Ichimoto, and I. Tohmura, The 17-month periodicity of sunspot activity, *Sol. Phys.*, *112*, 313–316, 1987.

Bame, S. J., D. J. McComas, D. T. Young, and R. D. Belian, Diagnostics of space plasmas, *Rev. Sci. Instrum.*, *57*, 1711–1716, 1986.

Behannon, K. W., M. H. Acuna, L. F. Burlaga, R. P. Lepping, N. F. Ness, and F. M. Neubauer, Magnetic field experiment for Voyager 1 and 2, *Space Sci. Rev.*, *21*, 235–257, 1977.

Belmont, A. D., D. G. dart, and M. S. Ulstad, The 10.7-cm solar flux and the 26-month oscillation, *J. Atm. Sci.*, *23*, 314–319, 1966.

Bridge, H. S., J. W. Belcher, R. J. Butler, A. J. Lazarus, A. M. Mavretic, J. D. Sullivan, G. L. Siscoe, and V. M. Vasyliunas, The plasma experiment on the 1977 Voyager mission, *Space Sci. Rev.*, *21*, 259–287, 1977.

Chapman, S., Notes on the solar corona and the terrestrial ionosphere, smithsonian contr., *Astrophys.*, *2*, 1, 1957.

Coates, A. J., et al., The electron spectrometer for the Cassini spacecraft, *J. Brit. Inter. Soc.*, *45*, 387–392, 1992.

Couzens, D. A., and J. H. King, *Interplanetary Medium Data Book - Supplement 3*, Nat. Space Sci. Data Cent., Goddard Space Flight Cent., Greenbelt, M, USA, 1986.

Cranmer, S. R., Coronal holes and the high-speed solar wind, *Space Sci. Rev.*, *101*, 229–294, 2002.

Crooker, N. U., and K. I. Gringauz, On the low correlation between long-term averages of solar wind speed and geomagnetic activity after 1976, *J. Geophys. Res.*, *98*, 59–62, 1993.

Crooker, N. U., J. Feynman, and J. T. Gosling, On the high correlation between long-term averages of solar wind speed and geomagnetic activity, *J. Geophys. Res.*, *82*, 1933–1937, 1977.

Fligge, M., S. K. Solanki, and J. Beer, Determination of solar cycle length variations using the continuous wavelet transform, *Astron. Astrophys.*, *346*, 313–321, 1999.

Fox, P., P. McIntosh, and P. R. Wilson, Coronal holes and the polar field reversal, *Sol. Phys.*, *177*, 375–393, 1998.

Frank, L. A., B. G. Burek, K. L. Ackerson, J. H. Wolfe, and J. D. Mihalov, Plasmas in Saturn's magnetosphere, *J. Geophys. Res.*, *85*, 5695–5708, 1980.

Gazis, P. R., Physics of the outer heliosphere, *Rev. Geophys.*, *29*, 955–961, 1991.

Gazis, P. R., Long term enhancements in solar wind speed, *J. Geophys. Res.*, *101*, 415–424, 1996a.

Gazis, P. R., Solar cycle variations in the heliosphere, *Rev. Geophys.*, *34*, 379–402, 1996b.

Gazis, P. R., J. D. Richardson, and K. I. Paularena, Long term periodicity in solar wind velocity during the last three solar cycles, *Geophys. Res. Lett.*, *22*, 1165–1168, 1995.

Gosling, J. T., Coronal mass ejections and magnetic flux ropes in interplanetary space, *Geophys. Monog.*, *58*, 343–364, 1990.

Gosling, J. T., The solar flare myth, *J. Geophys. Res.*, *98*, 18,937–18,949, 1993.

Gosling, J. T., Corotating and transient solar wind flows in three dimensions, *Annu. Rev. Astron. Astrophys.*, *34*, 35–73, 1996.

Gosling, J. T., Coronal mass ejections: An overview, *Geophys. Monog.*, *99*, 9–16, 1997.

Gosling, J. T., The solar wind, in *Encyclopedia of the Solar System*, edited by P. Weismann, L. McFadden, and T. Johnson, Academic Press, USA, 1999.

Gosling, J. T., J. R. Asbridge, S. J. Bame, and W. C. Feldman, Effects of a long entrance aperture upon the azimuthal response of spherical section electrostatic analyzers, *Rev. Sci. Instrum.*, *49*, 1260–1268, 1978.

Gosling, J. T., M. F. Thomsen, and R. C. Anderson, *A Cookbook for Determining Essential Transmission Characteristics of Spherical Section Electrostatic Analysers, Los Alamos National Laboratory Report LA-12962-MS*, Los Alamos National Laboratory, New Mexico, USA, 1984.

Hale, G. E., On the possible existence of a magnetic field in sunspots, *Astrophys. J.*, *28*, 315, 1908.

Hannula, H., IBS/CAPS cassini flight model, delivery data package of the mechanics, *Tech. rep.*, VTT Automation Space technology, 1994.

Holter, O., Wavelet analysis of time series, in *Proc. of the Cluster Workshop on Data Analysis Tools, Germany 28-30 Sept. 1994*, pp. 43–50, ESA SP-371, Braunschweig, Germany, 1995.

Howe, R., J. Christensen-Dalsgaard, F. Hill, R. W. Komm, R. M. Larsen, J. Schou, M. J. Thompson, and J. Toomre, Dynamic variations at the base of the solar convection zone, *Science*, *287*, 2456–2460, 2000.

Ichimoto, K., J. Kubota, M. Suzuki, I. Tohmura, and H. Kurokawa, Periodic behavior of solar flare activity, *Nature*, *360*, 422–424, 1985.

Kane, M., R. B. Decker, B. H. Mauk, and S. M. Krimigis, The solar wind velocity determined from voyager 1 and 2: Low-energy charged particle measurements in the outer heliosphere, *J. Geophys. Res.*, *103*, 267–276, 1998.

Kato, C., F. Mcdonald, and S. Yasue, Long–term periodic variations (1.8 year) of cosmic rays in the outer heliosphere, in *Proc. of ICRC 2001*, pp. 3589–3591, 2001.

King, J., *Interplanetary medium data book*, National Space Science Data Center preprint NSSDC/WDC-A-R&S 77-04, and supplements 1–5, 1977.

Kivelson, M. G., and C. T. Russell, *Introduction to Space Physics*, Cambridge University Press, New York, USA, 1995.

Kohlhase, C. E., and P. A. Penzo, Voyager mission description, *Space Sci. Rev.*, *21*, 77–101, 1977.

Koskinen, H., *Johdatus Plasmafysiikkaan ja sen Avaruussovellutuksiin*, Limes ry, Kruunuhaka, Finland, 2001.

Krivova, N. A., and S. K. Solanki, The 1.3-year and 156-day periodicities in sunspot data: Wavelet analysis suggest a common origin, *Astron. Astrophys.*, *394*, 701–706, 2002.

Lagoutte, D., J. C. Cerisier, J. L. Plagnaud, J. P. Villain, and B. Forget, High-latitude ionospheric electrostatic turbulence studied by means of the wavelet transform, *J. Atm. Terr. Phys.*, *54*, 1283–1293, 1992.

Lazarus, A. J., and R. L. McNutt, Jr, Low-energy plasma ion observations in Saturn's magnetosphere, *J. Geophys. Res.*, *88*, 8831–8846, 1983.

Linder, D. R., A. J. Coates, R. D. Woodliffe, C. Alsop, A. D. Johnstone, M. Grande, A. Preece, B. Narheim, and D. T. Young, The Cassini CAPS electron spectrometer, *Geophys. Monog.*, *102*, 257–262, 1998.

Lockwood, M., Long-term variations in the magnetic fields of the sun and the heliosphere: Their origin, effects, and implications, *J. Geophys. Res.*, *106*, 16,021–16,038, 2001.

Mayaud, P. N., The aa indices: A 100-year series characterizing the magnetic activity, *J. Geophys. Res.*, *77*, 6870–6874, 1972.

Mayaud, P. N., *A hundred year series of geomagnetic data, 1868-1967, indices aa, storm sudden commencements*, vol. 33 of *IAGA Bull.*, INT. Union of Geod. and Geophys., Paris, 1973.

McComas, D. J., and S. J. Bame, Channel multiplier compatible materials and lifetime tests, *Rev. Sci. Instrum.*, *55*, 463–467, 1984.

McComas, D. J., and J. E. Nordholt, New approach to 3-D, high sensitivity, high mass resolution space plasma composition measurements, *Rev. Sci. Instrum.*, *61*, 3095–3097, 1990.

McComas, D. J., J. R. Baldonado, S. J. Bame, and B. L. Barraclough, Channel electron multiplier compatibility with Viton and Apiezon-L vacuum grease, *Rev. Sci. Instrum.*, *58*, 2331–2332, 1987.

McComas, D. J., J. E. Nordholt, J. J. Berthelier, J. M. Illiano, and D. T. Young, The Cassini ion mass spectrometer, *Geophys. Monog.*, *102*, 187–193, 1998.

McIntosh, P. S., R. J. Thompson, and E. C. Willock, A 600–day periodicity in solar coronal holes, *Nature*, *360*, 322–324, 1992.

Mursula, K., and B. Zieger, The 13.5-day periodicity in the sun, solar wind and geomagnetic activity: The last three solar cycles, *J. Geophys. Res.*, *101*, 27,077–27,090, 1996.

Mursula, K., and B. Zieger, Simultaneous occurrence of mid-term periodicities in solar wind speed, geomagnetic activity and cosmic rays, in *Proc. of the Cosmic Ray Conference, Utah, 17.-25. 8. 1999*, pp. (7)123–(7)126, 1999.

Mursula, K., and B. Zieger, The 1.3–year variation in solar wind speed and geomagnetic activity, *Adv. Space Res.*, *25*, 1939–1942, 2000.

Mursula, K., T. Hiltula, and B. Zieger, Latitudinal gradients of solar wind speed around the ecliptic: Systematic displacement of the streamer belt, *Geophys. Res. Lett.*, *29*, 28–1–4, 2002.

Nevanlinna, H., and E. Kataja, An extension of the geomagnetic activity index series aa for two solar cycles (1844-1868), *Geophys. Res. Lett.*, *20*, 2703–2706, 1993.

Nevanlinna, H., and A. Ketola, *Magnetic results from Helsinki magnetic-meteorological observatory, Part III, Declination 1854-1880, Geomagnetic activity 1844-1880*, vol. 33 of *Geophysical Publications*, Finnish Meteorological Institute, Helsinki, 1993.

Nordholt, J. E., et al., The Cassini ion mass spectrometer: Performance metrics and techniques, *Geophys. Monog.*, *102*, 209–214, 1998.

Özgüç, A., and T. Ataç, Periodic behavior of solar flare index during solar cycles 20 and 21, *Sol. Phys.*, *123*, 357–365, 1989.

Parker, E. N., Dynamics of the interplanetary gas and magnetic fields, *Astrophys. J.*, *128*, 664–675, 1958.

Parker, E. N., A history of early work on the heliospheric magnetic field, *J. Geophys. Res.*, *106*, 15,797–15,801, 2001.

Paularena, K. I., A. Szabo, and J. D. Richardson, Coincident 1.3–year periodicities in the *ap* geomagnetic index and solar wind, *Geophys. Res. Lett.*, *22*, 3001–3004, 1995.

Pesses, M. E., W. V. Jones, and M. Forman, Voyager and pioneer missions to the boundaries of the heliosphere, *J. Geophys. Res.*, *98*, 15,123–15,127, 1993.

Press, W. H., B. P. Flannery, S. A. Teukolsky, and W. T. Vetterling, *Numerical Recipies, The Art of Scientific Computing*, Cambridge University Press, Cambridge, 1986.

Rangarajan, G. K., and L. M. Barreto, Long term variability in solar wind velocity and IMF intensity and the relationship between solar wind parameters & geomagnetic activity, *Earth Planets Space*, *52*, 121–132, 2000.

Richardson, J. D., Thermal ions at Saturn: Plasma parameters and implications, *J. Geophys. Res.*, *91*, 1381–1389, 1986.

Richardson, J. D., K. I. Paularena, J. W. Belcher, and A. J. Lazarus, Solar wind oscillations with 1.3 year period, *Geophys. Res. Lett.*, *21*, 1559–1560, 1994.

Rieger, E., G. Kanbach, C. Reppin, G. H. Share, D. J. Forrest, and E. L. Chupp, A 154-day periodicity in the occurrence of hard solar flares?, *Nature*, *312*, 623–625, 1984.

Scherer, K., H. Fichtner, E. Marsch, N. Shrivastava, and R. Schwenn, *The Outer Heliosphere: Beyond the Planets*, Copernicus Gesellschaft e.V., Katlenburg-Lindau, FRG, 2000.

Schreiber, H., On the periodic variations of geomagnetic activity indices Ap and ap, *Ann. Geophysicae*, *16*, 510–517, 1998.

Silverman, S. M., and R. Shapiro, Power spectral analysis of auroral occurrence frequency, *J. Geophys. Res.*, *88*, 6310–6316, 1983.

Sittler, E. C., Jr, Real-time spectral analysis algorithm for space plasma three-dimensional ion mass spectrometer, *Rev. Sci. Instrum.*, *64*, 2771–2781, 1993.

Smith, E. J., L. Davis, D. E. Jones, P. J. Coleman, D. S. Colburn, P. Dyal, C. P. Sonett, and A. M. A. Frandsen, The planetary magnetic field and magnetosphere of Jupiter: Pioneer 10, *J. Geophys. Res.*, *79*, 3501–3513, 1974.

Stamper, R., M. Lockwood, M. N. Wild, and T. D. G. Clark, Solar causes of the long-term increase in geomagnetic activity, *J. Geophys. Res.*, *104*, 28,325–28,342, 1999.

Suess, S. T., The heliopause, *Rev. Geophys.*, *28*, 97–115, 1990.

Torrence, C., and G. P. Compo, A practical guide to wavelet analysis, *Bulletin of the American Meteorological Society*, *79*, 61–78, 1998.

Valdes-Galicia, J. F., R. Perez-Enriquez, and J. A. Otaola, The cosmic–ray 1.68–year variation: a clue to understand the nature of the solar cycle?, *Sol. Phys.*, *167*, 409–417, 1996.

Vasyliunas, V. M., J. R. Kan, G. L.Siscoe, and S. I. Akasofu, Scaling relations governing magnetospheric energy transfer, *Planet. Space Sci.*, *30*, 359–365, 1982.

Vilppola, J. H., *Licentiate thesis: Cassini Mission and the CAPS/IBS Instrument*, University of Oulu, Department of Physical Sciences, Oulu, Finland, 1998.

Vilppola, J. H., P. J. Tanskanen, and B. L. Barraclough, Magnetospheric research with advanced techniques: Simulations of a spherical section electrostatic analyser, in *Proc. of the Ninth COSPAR Colloquim, Beijing, China, 1996*, vol. 9, pp. 75–84, Elsevier Science Ltd, Oxford, England, 1998.

von Steiger, R., History of the solar wind, in *Proc. Session G6.01 of the IAGA-IASPEI Joint Scientific Assembly, Hanoi Vietnam, 18-30 Aug. 2001*, Elsevier Science, Submitted 2002.

Wang, Y. M., and N. R. Sheeley, Jr, Solar wind speed and coronal flux-tube expansion, *Astrophys. J.*, *355*, 726–732, 1990.

Wang, Y. M., J. Lean, and N. R. Sheeley, Jr, The long-term variation of the sun's open magnetic field, *Geophys. Res. Lett.*, *27*, 505–508, 2000.

Wolfe, J. H., J. D. Mihalov, H. R. Collard, D. D. McKibbin, L. A. Frank, and D. S. Intriligator, Pioneer 10 observations of the solar wind interaction with Jupiter, *J. Geophys. Res.*, *79*, 3489–3500, 1974.

Yacob, A., and B. N. Bhargava, On 26-month periodicity in quiet-day range of geomagnetic horizontal force and in sunspot number, *J. Atm. Terr. Phys.*, *30*, 1907–1911, 1968.

Ylikorpi, T., and T. Luntama, *Development of an actuator for CAPS instrument on spacecraft Cassini, ESA SP-374*, pp. 97–101, European Space Agency, 1995.

Young, D. T., and N. Eaker, *Cassini Plasma Spectrometer (CAPS), Confirmation Review*, Southwest Research Institute and Jet Propulsion Laboratory, San Antonio, Texas, 1991.

Young, D. T., and P. A. Jensen, CAPS interface control document, *Tech. rep.*, Southwest Research Institute, 1993.

Young, D. T., S. J. Bame, M. F. Thomsen, R. H. Martin, J. L. Burch, and J. A. M. B. Reinhard, 2π-radian field-of-view toroidal electrostatic analyser, *Rev. Sci. Instrum.*, *59*, 743–751, 1988.

Young, D. T., et al., *A proposal for the Plasma Science (PLS) investigation for the Cassini orbiter spacecraft, Volyme 1: Investigation and technical plan, SwRI Proposal 15-9376*, Southwest Research Institute, San Antonio, Texas, 1989.

Young, D. T., et al., Cassini plasma spectrometer investigation, in *The International Society for Optical Engineering, 5-6 August 1996, Denver, Colorado, Cassini/Huygens: A Mission to the Saturnian System*, no. 2803 in SPIE Proceedings series, pp. 118–128, Soc. of Photo-Optical Instrumentation Engineers, Bellingham, Washington, USA, 1996.

Young, D. T., et al., Cassini Plasma Spectrometer Investigation, *Geophys. Monog.*, *102*, 237–242, 1998.

Young, D. T., et al., Cassini Plasma Spectrometer Investigation, *submitted to Space Sci. Rev.*, 2003.